

**Structural Geology and Geochronology of the  
Bernic Lake Area in the Bird River Greenstone  
Belt, Manitoba: Evidence for Syn-Deformational  
Emplacement of the Bernic Lake Pegmatite  
Group**

by

Paul Kremer

A thesis  
presented to the University of Waterloo  
in fulfillment of the  
thesis requirement for the degree of  
Master of Science  
in  
Earth Sciences

Waterloo, Ontario, Canada, 2010

© Paul Kremer 2010

## **Author's Declaration**

I hereby declare that I am the sole author of this thesis. This is a true copy of the thesis, including any required final revisions, as accepted by my examiners.

I understand that my thesis may be made electronically available to the public.

## Abstract

The Bernic Lake Formation in the Bird River greenstone belt consists dominantly of mafic to felsic arc volcanic and volcanoclastic rocks, with varying amounts of mafic to felsic intrusive rocks, including the Bernic Lake pegmatite group. U-Pb geochronological analyses on selected samples around the Bernic Lake area, indicate that the Tanco gabbro, the Birse Lake granodiorite and the volcanic rocks of the Bernic Lake Formation are contemporaneous ca. 2724 and form part of a singular volcanic and subvolcanic complex. The highly evolved, LCT-type, rare element-bearing Bernic Lake pegmatite group, including the world class Tanco pegmatite, was emplaced in the Bernic Lake Formation during a belt-scale tectonomagmatic event associated with  $G_3$  deformation between ca. 2650 and 2640 Ma.

Early and rarely preserved isoclinal folding in the Bernic Lake Formation attributed to  $G_1$  deformation was followed north-south directed compression resulting in refolding and transposition of  $G_1$  structures by east-west trending upright  $F_2$  folds. Continued compression caused strain localization and south-side-up shearing along the North Bernic Lake Shear Zone (NBLSZ), which juxtaposes MORB-like basalt of the south panel to the south against arc volcanic and volcanoclastic rocks of the Bernic Lake Formation to the north.  $G_3$  deformation is characterized by a spaced  $S_3$  fracture cleavage that overprints the penetrative  $S_2$  fabric, and dextral reactivation of the NBLSZ. Pegmatitic melt ascended from depth along the reactivated NBLSZ during this time and was emplaced both within the shear zone and within rock units adjacent to it. The shapes and orientations of the pegmatites are controlled in part by the rheology of the host rocks into which they were emplaced. Rheologically competent lithologies responded to  $G_3$  strain by brittle fracture and the pegmatites occurring therein are flat and tabular; rheologically incompetent lithologies responded to  $G_3$  strain by ductile-brittle deformation and the pegmatites therein are irregular, folded, and/or boudinaged. The contrasting styles suggest that the pegmatites intruded while the rocks of the Bernic Lake Formation were at or near the brittle-ductile transition.

## Acknowledgements

Remembering to thank everyone involved in helping you through a process like this seems a daunting task. The list continues to grow in a seemingly exponential manner. Firstly, I would like to offer my sincerest thanks to my advisors, Drs. Shoufa Lin and Robert Linnen. For their guidance, their enthusiasm, their support and their patience as I worked my way through this project, I am most grateful.

I would also like to thank the Manitoba Geological Survey, in particular Paul Gilbert and Tim Corkery. They were always willing and excited to discuss my findings and answer my questions (more often than not causing me to contemplate new ones in the process). Their knowledge with respect to the geology of Manitoba seems almost as limitless as their zeal to continue looking at the rocks and further unraveling the stories that they hold. The logistical and financial support that the survey provided was also critical to the success of the project.

In addition to financial support provided by the Tantalum Mining Corporation of Canada Ltd. (Tanco), I was also given unlimited and invaluable right of entry to the Tanco Mine over the course of study. This applied not only to the extensive drill core library and underground workings, but also to the employees like Peter Vanstone, Carey Galeschuk, and Shane Moran who would always take the time to talk with me and assist me in any way that they could.

I consider Don Davis at the Jack Satterley Geochronology Laboratory to be a master of his craft. The data he returned from the samples that I submitted were of the highest quality, and the conclusions that the results helped me to reach would have been impossible without.

Finally, I would like to thank the students at the University of Waterloo whom have become dear friends over the past few years. I especially appreciate everything that Jen Parks and the rest of the Shoufa Squad have done for me and helped me with, both with regards to work and with regards to life.

# Table of Contents

<b>Author's Declaration</b>	<b>ii</b>
<b>Abstract</b>	<b>iii</b>
<b>Acknowledgements</b>	<b>iv</b>
<b>Table of Contents</b>	<b>v</b>
<b>List of Figures</b>	<b>vii</b>
<b>List of Tables</b>	<b>ix</b>
<b>CHAPTER 1 Introduction</b>	<b>1</b>
<b>1.1 Scope and Purpose</b>	<b>1</b>
<b>1.2 Location, Access, and Topography</b>	<b>2</b>
<b>1.3 Collaborations</b>	<b>3</b>
<b>CHAPTER 2 Geology of the Bird River Greenstone Belt</b>	<b>5</b>
<b>2.1 Previous Work</b>	<b>5</b>
<b>2.2 Geology and Tectonic Framework of the Western Superior Province</b>	<b>7</b>
<b>2.3 Geology of the Bird River Greenstone Belt</b>	<b>10</b>
2.3.1 Stratigraphy and structural geology	12
2.3.1.1 <i>Eaglenest Lake Formation</i>	12
2.3.1.2 <i>South panel MORB-type basalt</i>	13
2.3.1.3 <i>Bernic Lake Formation</i>	13
2.3.1.4 <i>North panel MORB-type basalt</i>	15
2.3.1.5 <i>Diverse arc assemblage</i>	15
2.3.1.6 <i>Peterson Creek Formation</i>	16
2.3.1.7 <i>Booster Lake Formation</i>	17
2.3.1.8 <i>Flanders Lake Formation</i>	18
2.3.2 Intrusive rocks	19
<b>CHAPTER 3 Geology and Structure of the Bernic Lake Area</b>	<b>22</b>
<b>3.1 Introduction</b>	<b>22</b>
<b>3.2 Geology of the Bernic Lake Area</b>	<b>23</b>
3.2.1 Southern panel MORB-type basalt	23
3.2.2 Bernic Lake Formation	25
3.2.3 Booster Lake Formation	28

3.2.4 Tanco gabbro	29
3.2.5 Birse Lake granodiorite	29
3.2.6 Bernic Lake pegmatite group	31
<b>3.3 Structural Geology of the Bernic Lake Area</b>	<b>31</b>
3.3.1 G <sub>1</sub> structures	33
3.3.2 G <sub>2</sub> structures	33
3.3.3 G <sub>3</sub> structures	39
3.3.4 G <sub>4</sub> structures	41
3.3.5 Late, brittle deformation	46
<b>3.4 Relationship of the Bernic Lake Pegmatite Group to Structural Elements</b>	<b>48</b>
<b>CHAPTER 4 U-Pb Geochronology of the Bernic Lake Area</b>	<b>52</b>
<b>4.1 Introduction</b>	<b>52</b>
<b>4.2 Analytical Techniques</b>	<b>52</b>
4.2.1 Sample processing and mineral separation	53
<b>4.3 Sample Description and U-Pb Results</b>	<b>53</b>
4.3.1 Sample PK-05-1081	53
4.3.2 Sample PK-06-1250	54
4.3.3 Sample PK-06-1197	63
4.3.4 Sample PK-05-1050	66
4.3.5 Sample PK-06-1251	72
<b>4.4 Interpretation of U-Pb Geochronology Data</b>	<b>72</b>
<b>CHAPTER 5 Emplacement model for the Bernic Lake Pegmatite Group</b>	<b>76</b>
<b>5.1 Structural Associations of the Bernic Lake Pegmatite Group</b>	<b>76</b>
<b>5.2 Temporal Associations of the Bernic Lake Pegmatite Group</b>	<b>79</b>
<b>5.3 Emplacement Model for the Bernic Lake Pegmatite Group</b>	<b>80</b>
<b>5.4 Summary</b>	<b>84</b>
<b>References</b>	<b>85</b>
<b>Appendix 1</b>	<b>Map in back pocket</b>
Geology of the Bernic Lake Area, Bird River Greenstone Belt, Manitoba	

## List of Figures

<b>Figure 1.</b> Simplified geological map of the Western superior Province	8
<b>Figure 2.</b> Simplified geological map of the Bird River greenstone belt	11
<b>Figure 3.</b> Outcrop photographs of the south panel MORB-type basalt	24
<b>Figure 4.</b> Outcrop photographs of the Bernic Lake Formation	27
<b>Figure 5.</b> Outcrop photographs of the Tanco gabbro	30
<b>Figure 6.</b> Geology of the Bernic Lake area showing the approximate location of pegmatites in the Bernic Lake pegmatite group	32
<b>Figure 7.</b> Rarely preserved isoclinal $F_1$ fold refolded by upright $F_2$ fold	34
<b>Figure 8.</b> Lower hemisphere equal area plot showing the orientations of $G_2$ fabric elements in the Bernic Lake area	36
<b>Figure 9.</b> Upright folds in the albitic aplite zone, underground at the Tanco mine	38
<b>Figure 10.</b> Outcrop photographs of kinematic indicators in the North Bernic Lake shear zone	40
<b>Figure 11.</b> Outcrop photograph showing oblique relationship between $S_2$ and $S_3$ in the Bernic Lake Formation	42
<b>Figure 12.</b> Photographs showing the mutually overprinting relationship of opposing senses of slip along conjugate fracture planes in the Tanco mine	44
<b>Figure 13.</b> Lower hemisphere equal area stereonet showing the orientation of the conjugate fracture set along which the Tanco pegmatite intruded	45
<b>Figure 14.</b> Rose diagram showing the orientations of late, post-tectonic fractures in the Bernic Lake area	47
<b>Figure 15.</b> Outcrop photographs of the Oompa Loompa pegmatite emplaced within the NBLSZ east of Bernic Lake	49
<b>Figure 16.</b> Photos taken underground at the Tanco mine showing the relationship of the Tanco pegmatite to the various generations of fractures	50
<b>Figure 17.</b> Electron microprobe BSE images of zircons collected from sample PK-05-1081	56

<b>Figure 18.</b> Concordia diagram showing ID-TIMS data and photomicrographs of zircon collected from sample PK-06-1081	57
<b>Figure 19.</b> $^{207}\text{Pb}/^{206}\text{Pb}$ age data from TE-TIMS analyses on zircon from sample PK-05-1081	58
<b>Figure 20.</b> Concordia diagram showing ID-TIMS data from zircon collected from sample PK-06-1250	61
<b>Figure 21.</b> $^{207}\text{Pb}/^{206}\text{Pb}$ age data (corrected) from TE-TIMS analyses on zircon from sample PK-06-1250	62
<b>Figure 22.</b> Concordia diagram showing ID-TIMS data from zircon collected from sample PK-06-1197	65
<b>Figure 23.</b> Photomicrographs and electron microprobe BSE images showing zircon collected from sample PK-05-1050	67
<b>Figure 24.</b> $^{207}\text{Pb}/^{206}\text{Pb}$ age data (corrected) from TE-TIMS analyses on zircon and cassiterite (lower right) from sample PK-05-1050	69
<b>Figure 25.</b> Concordia diagram showing ID-TIMS data from columbite collected from sample PK-05-1050 and PK-06-1251	71
<b>Figure 26.</b> Simplified geological map of the Bird River greenstone belt showing the spatial association of 6 pegmatite groups of the Winnipeg River pegmatite field to major, formation-bounding shear zones	77
<b>Figure 27.</b> Schematic diagram showing the development of structures during $G_{2-4}$ deformation and the emplacement of the Bernic Lake pegmatite group	83

## List of Tables

<b>Table 1.</b> ID-TIMS data from sample PK-05-1081	55
<b>Table 2.</b> ID-TIMS data from sample PK-06-1251	60
<b>Table 3.</b> ID-TIMS data from sample PK-06-1197	64
<b>Table 4.</b> ID-TIMS data from sample PK-05-1050	70
<b>Table 5.</b> ID-TIMS data from sample PK-06-1251	73

# CHAPTER 1

## Introduction

### 1.1 Scope and Purpose

The geology of the Bird River greenstone belt has not been examined in detail since the late 1970's (Cerny et al. 1981). The belt has been of great economic interest since the late 1920's owing to the presence of the layered mafic/ultramafic Bird River sill, which contains numerous Ni-Cu-PGE prospects including the past-producing Maskwa and Dumbarton mines, as well as Winnipeg River pegmatite field, containing abundant rare-element bearing pegmatites. A veritable cornucopia of scientific research has been conducted on pegmatitic intrusions within the belt, however, the work to date has largely addressed their classification, geochemistry, mineral chemistry, and petrogenesis (e.g. Cerny 1972a, 1972b, 1974, 1978, 1990, 1991; Cerny and Bristol 1972; Cerny and Turnock 1971a, 1975; and Lenton 1979), with little emphasis placed on the tectonic controls of their emplacement (Brisbin 1986).

The purpose of this thesis is three-fold. Firstly, it is designed to examine and map in detail the geology and structure of the Bernic Lake area to update existing maps (Chapter 3), including constraining the genetic and temporal relationships of various lithologies in the area using U-Pb geochronology (Chapter 4). The Bernic Lake area was chosen specifically for study, as it hosts the Bernic Lake pegmatite group, of which the highly-fractionated, complex, and currently producing (Li, Ce, and Ta) LCT-type Tanco pegmatite is most noteworthy. However, the timing and emplacement mechanisms of these economically significant pegmatites are poorly understood within the local and belt-scale tectonic framework. The second purpose of this study is to place structural and

temporal constraints on the emplacement of the Bernic Lake pegmatite group with respect to the newly defined tectonostratigraphic framework of the area (Chapter 5). Finally, the data and interpretations of this study are integrated into concurrent belt-scale studies of the stratigraphy (Gilbert 2006, 2007), structural geology (Duguet et al. 2005, 2006), and geodynamics (Duguet 2007) of the Bird River greenstone belt as a whole and its place in the overall evolution of the Superior Province.

In order to accomplish the above goals, geological mapping of the area around Bernic Lake was undertaken at a scale of 1:10,000 with specific emphasis placed on examining the various generations of macro-, meso-, and micro-scale structures and fabric elements within the rocks to develop a tectonic model for the area based on the overprinting relationships between them. Detailed investigations of exposed pegmatites in the Bernic Lake pegmatite group were conducted and particular attention was paid to their relationships and attitudes with respect to the above defined fabric elements. Pegmatites not exposed at surface were studied by examining diamond drill core (both exploration and production) and underground mapping at the Tanco mine. Wherever possible, samples were collected for thin section analysis. Selected outcrops were also sampled for U-Pb geochronological analysis to constrain the absolute timing of events, including volcanism, intrusion, and deformation.

## **1.2 Location, Access, and Topography**

The Bird River greenstone belt is located approximately 130 km northeast of Winnipeg near the towns of Lac du Bonnet and Pinawa, Manitoba. It is easily accessible by road from Winnipeg via Highway 59 and Provincial Roads 212, 313, 314, and 315.

Access to the northwestern corner of Bernic Lake is achieved via the Tanco mine road. The remainder of Bernic Lake is reached by boat; traversing is required to access internal ground lying away from the shore.

The topography of the area is typical of the southwestern Canadian Shield, consisting of a series of low-lying ridges of lichen-covered outcrop (in this case east-west trending), separated by tree-covered ground, valleys, muskeg, and swamps that mimic in part the underlying geology.

### **1.3 Collaborations**

This thesis is one segment of a multidisciplinary study that was initiated by the Manitoba Geological Survey and the University of Waterloo with participation from industry sponsors to update and increase the geological knowledge of the Bird River greenstone belt and the known and potential mineral deposits that occur therein. The individual goals and principal researchers of each sub-study are outlined below:

- 1) Detailed supracrustal stratigraphy and geochemistry (P. Gilbert, Manitoba Geological Survey)
- 2) Structural geology and tectonic history (M. Duguet PDF, University of Waterloo)
- 3) Structure and timing of the Bernic Lake rare element-bearing pegmatites (P. Kremer, this study)
- 4) Nature of Ni-Cu-PGE mineralization in the Bird River sill (C. Mealin, University of Waterloo)

Funding for the various aspects of the project was provided by NSERC and also by various mining and exploration companies currently active in the Bird River

greenstone belt (Tantalum Mining Corporation of Canada Ltd., Gossan Resources Ltd.,  
Mustang Minerals Ltd.).

## CHAPTER 2

### Geology of the Bird River Greenstone Belt

#### 2.1 Previous Work

Early workers in the belt include Tyrrell (1900) and Moore (1913), the latter of whom correlated the volcano-sedimentary sequences of the Bird River greenstone belt to those found in the Rice Lake greenstone belt of the Uchi domain to the north (Cerny et al. 1981). In the early 1920's, Ni-Cu sulphide was discovered around Cat Lake and resulted in widespread prospecting, the ensuing discovery of numerous rare-metal bearing pegmatites of the Cat Lake-Winnipeg River pegmatite field (including the Tanco pegmatite in 1929), and subsequent tin mining ventures (Jack Nutt Mines) around Bernic and Shatford lakes over the next decade (Vanstone et al. 2002); many of the pegmatites were also explored for lithium and molybdenum. Springer and Davies conducted regional and detailed geological mapping of selected areas in the belt (Cat Lake, Booster Lake, Bird Lake, Shatford Lake) through the 1950's culminating in a series of publications with regards to the pegmatite field (Springer 1949, 1950; Davies 1952, 1955, 1956, 1957).

The Tantalum Mining Corporation of Canada Ltd. (Tanco) formed as a joint venture between Chemalloy Minerals Limited and Northern Goldfield Limited in 1967 after positive results were released from a tantalum market study conducted by Chemalloy (Vanstone et al. 2002). The Tanco mine began underground extraction of tantalum in 1969, and is currently producing lithium, tantalum, and cesium. Since then, detailed mineralogical and petrological studies of the Bird River belt pegmatites (and of the Tanco pegmatite in particular) have been conducted (Cerny 1972a, 1972b, 1974, 1978; Cerny and Bristol 1972; Cerny and Turnock 1971a, 1975; and Lenton 1979). Cerny

and Turnock (1971b) made the first efforts at classification of the various pegmatitic bodies within the field and their petrogenesis was addressed by Cerny and Turnock (1975), Cerny and Trueman (1977), Cerny et al. (1981), and Cerny (1990, 1991). London (1986) examined fluid inclusions in petalite, spodumene, and eucryptite and Morgan and London (1987) studied alteration haloes in the amphibolitic wallrocks around the Tanco pegmatite, both in attempts to constrain its P-T-t evolutionary path.

Regional studies were conducted by McRitchie (1971) and Trueman (1980), the latter of whom defined a detailed stratigraphy comprising 6 distinct volcanic and/or sedimentary sequences (Eaglenest Lake, Lamprey Falls, Peterson Creek, Bernic Lake, Flanders Lake, and Booster Lake formations). Geochronological studies have been carried out by Wang (1993), who examined U-Pb geochronology across the belt and Baadsgaard and Cerny (1993a, 1993b) who dated various pegmatites within the Cat Lake-Winnipeg River pegmatite field.

More recently, a collaborative effort involving government, academia, and industry has been undertaken to completely revisit the Bird River greenstone belt (Duguet et al. 2005, 2006, 2007; Gilbert 2005, 2006, 2007; Kremer 2005; Kremer and Lin 2006; and Mealin 2006). The project resulted in a new 1:20,000 scale geological map (Gilbert et al., 2008), an updated stratigraphy based on observed field relationships in conjunction with modern geochemical and geochronological techniques (Gilbert 2006, 2007), and an updated structural and geodynamic model (Duguet et al. 2006, 2007, 2009) and this study.

Mining and exploration activity in the Bird River greenstone belt continues for rare-element bearing pegmatites (Tanco) as well as Ni-Cu-PGE mineralization associated

with the Bird River sill (Mustang Minerals Ltd., Gossan Resources Ltd., Marathon PGM Corporation Ltd.).

## **2.2 Geology and Tectonic Framework of the Western Superior Province**

The Archean Superior Province of the Canadian Shield is the largest Archean craton in the world. The western Superior Province consists of a series of east-west trending, fault-bounded lithostratigraphic domains, each showing distinct lithological and structural characteristics (Card and Ciesielski 1986; Card 1990). Early subdivisions of the western Superior Province identified nine such subprovinces, alternating between granite-greenstone dominated (e.g. Uchi subprovince, Wabigoon subprovince, Wawa subprovince) and metasedimentary belts (e.g. English River subprovince, Quetico subprovince) (Card 1990; Thurston et al. 1991). However, research supported by detailed geochronology has allowed for internal subdivision of subprovinces into fault-bounded terranes and domains with detached tectonostratigraphic histories with respect to one another prior to amalgamation (Percival et al. 2006). Figure 1 shows the current subdivisions of the western Superior Province after Percival et al. 2006. Subprovinces, domains, and (super)terrane represent vestiges and fragments of ancient Mesoarchean continental and Neoarchean intra-oceanic crust accreted to the margins of core Mesoarchean microcontinental proto-cratons (represented by the 3.8 Ga Northern Superior superterrane, the 3.4 Ga Winnipeg River terrane, and the 3.0 Ga North Caribou superterrane) during 5 orogenic events (historically combined into the Kenoran

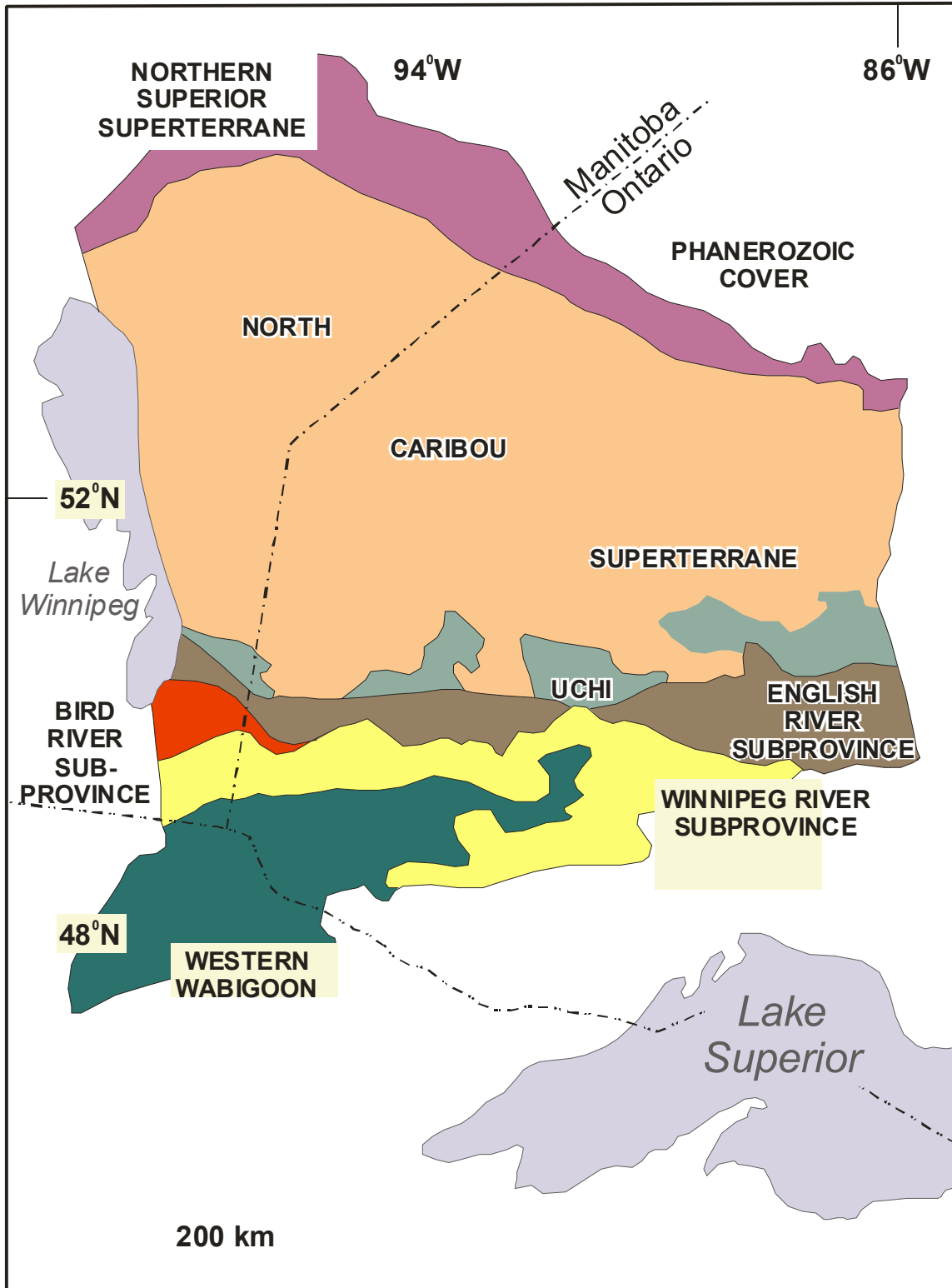


Figure 1. Simplified geological map of the Western Superior Province (Percival et al. 2006).

orogeny) spanning a 40 Ma period between approximately 2.72 and 2.68 Ga (Thurston et al. 1991, Percival et al. 2006).

Amalgamation of the Superior Province began with the Northern Superior orogeny (~2.72–2.71 Ga) which docked the Northern Superior superterrane with the North Caribou terrane (Percival et al. 2006). The granite-greenstone dominated Wabigoon terrane merged with the Winnipeg River terrane during the Central Superior orogeny at 2.715 Ga. The composite Superior terrane was formed when continued northward subduction of the Wabigoon – Winnipeg River superterrane under the southern margin of the North Caribou superterrane resulted in a collisional event (Uchian orogeny) and the deposition and subsequent burial of the syn-orogenic English River terrane sedimentary rocks. Similar north-vergent subduction during the Shebandowanian orogeny (~2.695 Ga) juxtaposed the Abitibi – Wawa terrane against the composite Superior terrane and also led to the deposition of the Quetico terrane accretionary wedge (Percival et al. 2006). Finally, the Minnesota River Valley terrane to the south collided with and was subducted under the composite Superior terrane in the ~2.68 Ga Minnesotan orogeny.

Younger episodes of regional deformation have also been reported, but are domainal and localized around accreted terrane boundaries, rather than manifest across the entire Superior Province. These events are attributed to continued oblique convergence post amalgamation of the various components of the Superior Province (Hrabi and Cruden 2006). Melnyk et al. (2006) described late dextral transpression resulting in a strong flattening fabric, steepening of older structures, and the rotation of pre-existing  $F_5$  fold axes around rigid intrusive rocks near the Winnipeg River

subprovince boundary. Syn-kinematic intrusions attributed to this event in the Vermillion Bay area were dated (Cruden et al. 1997), and suggest deformation as late as 2.65 Ga. Hrabi and Cruden (2006), interpret the oblique (dextral – S-side-up) Sydney Lake fault, which separates the English River terrane from the Uchi domain, as a late feature; it crosscuts the structural grain of the English River terrane on Lithoprobe seismic reflection profiles. Peraluminous granites and pegmatites that are deformed by a prominent S-C fabric associated with the fault yield ages of  $2663 \pm 7$  Ma (Turek et al. 1989) and shearing is thought to have continued until at least  $\sim 2.64$  Ga based on Ar-Ar studies (Hrabi and Cruden 2006). In the Bird River greenstone belt, Duguet et al. (2006) and this study have also noted significant deformation as young as 2.64 Ga on the basis of U-Pb data from syn-kinematic peraluminous granites and pegmatites (see Chapter 4).

### **2.3 Geology of the Bird River Greenstone Belt**

The Bird River greenstone belt lies in the western Superior Province and is flanked by the metasedimentary English River terrane to the north and the largely plutonic Winnipeg River terrane to the south (Figure 1). The Separation Lake greenstone belt represents the extension of the Bird River greenstone belt in Ontario. The Bird River greenstone belt comprises various sequences of metavolcanic and associated metasedimentary rocks intruded by multiple generations of mafic and felsic syn- and post-volcanic intrusive rocks (Figure 2). The belt has been subdivided into two (north and south) structural panels exhibiting distinct geochemical affinities and U-Pb ages, separated by the east-west trending Booster Lake Formation, a fault-bounded sequence of turbidites (Gilbert, 2006).

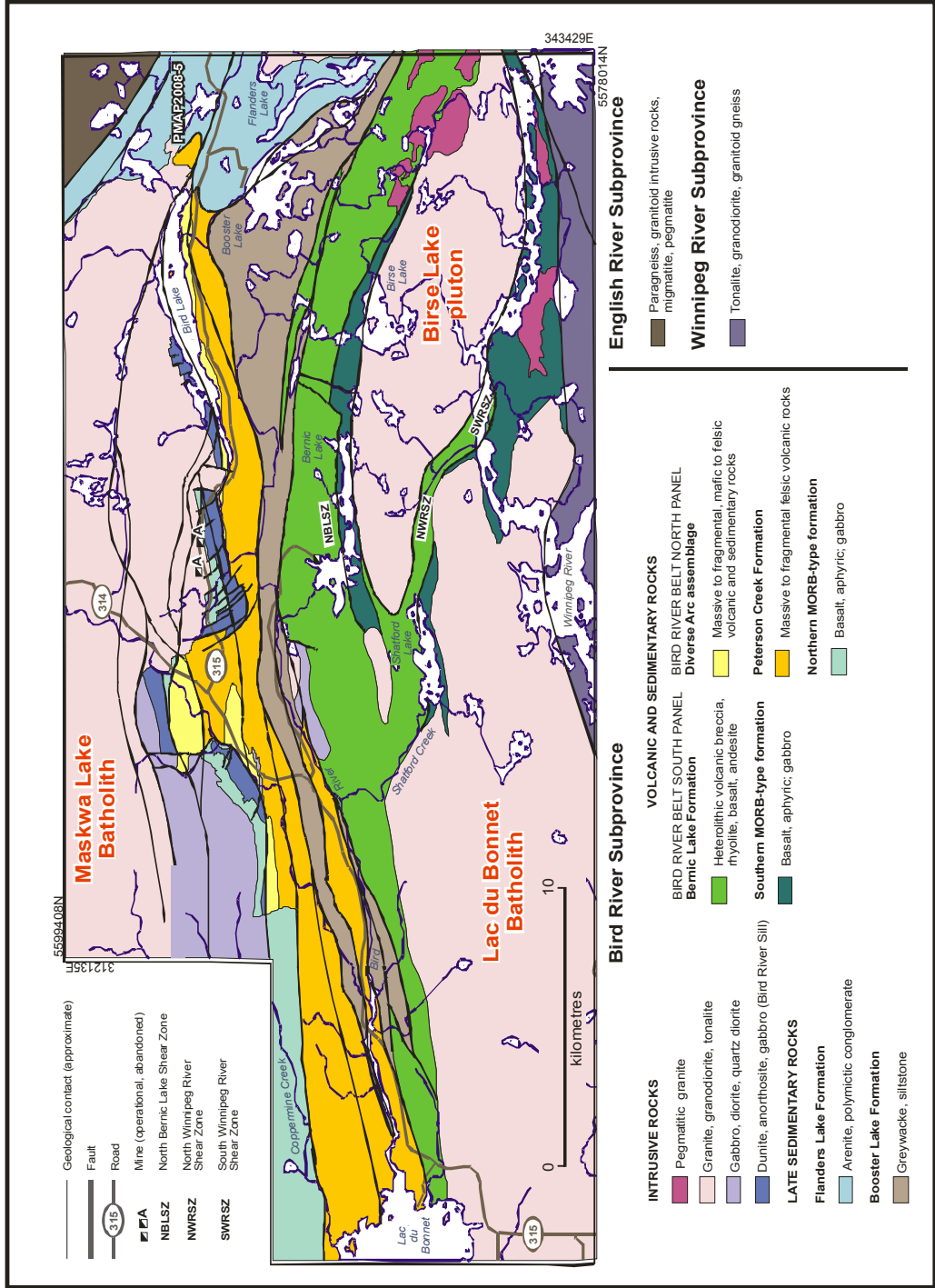


**Figure 2.** Simplified geological map of the Bird River greenstone belt (Gilbert, 2007). The study area for this thesis is located around Bernic Lake, in the centre of the area.

The geology and structure of the Bird River greenstone belt are synthesized below based on the most recent research in the area, including Duguet et al. (2005, 2006, 2007, 2009), Gilbert (2005, 2006, 2007), Gilbert et al., (2008), Kremer (2005), Kremer and Lin (2006), and Mealin (2005, 2006).

### **2.3.1 Stratigraphy and structural geology**

#### **2.3.1.1 Eaglenest Lake Formation**

The Eaglenest Lake Formation is located in the southern panel of the Bird River greenstone belt along the Winnipeg River and marks the southern margin of the supracrustal sequence (Cerny et al. 1981). It is a 600 m thick, south-facing sequence of turbiditic sediments. Rock types consist largely of crudely-bedded, steeply-dipping, poorly-sorted mafic volcanoclastic and pebbly wackes interbedded with quartzofeldspathic volcanoclastic sandstone (Trueman, 1980). Sediments range from fine- to coarse-grained and contain a prominent foliation; pebbles are flattened parallel to schistosity. Biotite schist and amphibolite occur to the south where the Eaglenest Lake Formation is pervasively intruded by plutonic rocks of the Winnipeg River terrane (Beakhouse, 1977). A unit of banded iron formation (chert-magnetite  $\pm$  pyrrhotite and pyrite) approximately 6 metres thick is limited to the northern margin of the formation where it is in fault contact with the south panel MORB-type basalt (Cerny et al. 1981). The temporal relationship between the Eaglenest Lake Formation and the south panel MORB-type basalt remains poorly constrained, and it is currently unclear where the Eaglenest Lake Formation fits in the overall stratigraphy of the belt.

### 2.3.1.2 South panel MORB-type basalt

MORB-type basalt (previously named Lamprey Falls Formation) in the south panel (Winnipeg River area) is composed largely of aphyric pillowed to massive basalt with MORB-type geochemical profiles. Pillows are well preserved and average 0.5-1 m across, though mega-pillows (1 x 5 m) have been reported (Gilbert 2006). Quartz-filled amygdales are common and are generally concentrated in zones towards the top of individual pillows. Younging criteria point north; however, in the western part of the sequence local reversals have been observed (Duguet et al. 2006). The effects of alteration, recrystallization, and grain coarsening are apparent throughout the sequence. Several units of banded iron formation (chert-magnetite) occur in the south panel. In one instance a unit of iron formation reaches up to 25 m in thickness and can be traced laterally for up to 500 m. Zones of pervasive alteration and associated pyrite-pyrrhotite-chalcopyrite mineralization locally occur immediately south of the iron formation (Duguet et al. 2006; Gilbert 2006).

### 2.3.1.3 Bernic Lake Formation

The Bernic Lake Formation forms part of the south panel of the Bird River greenstone belt (Gilbert 2007). It occurs as an approximately 2 km thick, fault-bounded sequence between the south panel MORB-type basalt to the south and the Booster Lake Formation to the north across the entire length of the belt (Gilbert 2006, 2007). Primary lithologies include mafic through to felsic volcanic rocks with calc-alkaline, continental arc-type affinities (Gilbert 2006). In the central portion of the belt around Bernic Lake, aphyric basalt with abundant quartz and feldspar amygdules is the dominant volcanic

phase (Kremer 2005; Kremer and Lin 2006), whereas massive to fragmental rhyolite and dacite predominate in the western portion (Gilbert 2007). Discontinuous lenses of heterolithic volcanic breccia and subordinate volcanoclastic sandstone are found throughout the Bernic Lake Formation. Silicate- and oxide-facies iron formation has been observed at two locations. Near the northern margin of the formation, bedded chert, carbonate, greywacke-siltstone, and amphibolite with local pyrite mineralization outcrops along the southern shore of Bird River and extends to Provincial Road 314. A single outcrop of tightly folded (west-plunging) silicate facies iron formation is located approximately 120 m south (Gilbert 2007).

The Bernic Lake Formation is interpreted by Gilbert (2007) to be north facing, though younging indicators in outcrop are rare owing to the effects of deformation and alteration. Occasionally, graded beds in volcanoclastic sandstone and locally well-preserved pillows agree with north younging. Furthermore, the volcanic rocks in the sequence become geochemically more evolved from south to north (Gilbert 2007), which also supports this interpretation. Evidence for folding, however, is present near the southern margin of the Bernic Lake Formation along the northern shore of Bernic Lake, where two outcrops show moderately convincing south facing features. Along the power line east of the Tanco mine, metre-scale folds with M-symmetry occur. Furthermore, in a well-exposed outcrop of heterolithic volcanic breccia located approximately 1 km north of Bernic Lake, bedding is rotated approximately 45° clockwise with respect to the dominant foliation (Kremer 2005); in most outcrops, bedding and foliation are sub-parallel.

#### 2.3.1.4 North panel MORB-type basalt

North panel MORB-type basalt comprises the oldest known rocks in the coherent stratigraphy of the northern panel of the Bird River greenstone belt (Gilbert 2007). Basalt consists largely of pillowed to massive, aphyric, basaltic flows that have mid-ocean ridge basalt (MORB-type) geochemical affinities (Gilbert, 2005). However, a 70 m thick distinctive unit of plagioclase megacrystic basalt with phenocrysts up to 5 cm is interlayered with aphyric flows. Flow breccia, tuff, hyaloclastite, and felsic volcanic units occur in limited amounts (Gilbert 2007); a single unit of banded iron formation (chert-magnetite-Fe sulphide assemblages) occurs in the north panel near the Dumbarton mine (Cerny et al. 1981). Northwest of the Bird River sill, gabbro is common and locally comprises over 30% (up to 90%) of the exposed south panel MORB-type basalt (Gilbert 2007). Where pillows are well preserved, younging criteria consistently point to the south.

#### 2.3.1.5 Diverse arc assemblage

The diverse arc assemblage, located south of the north panel MORB-type basalt, has an estimated thickness of approximately 750 m (Gilbert 2007). The lower part of the sequence contains turbidites and debris flows interlayered with chert and fine-grained mafic to felsic flows and tuffs. Volcanic rocks have calc-alkaline arc-type geochemical signatures (Gilbert 2006). A distinctive layer of polymictic conglomerate (~75 m thick) with clasts of unsorted basalt and gabbro with lesser rhyolitic, turbiditic, and chert clasts, overlies the lower sequence and acts as a marker horizon (Gilbert 2006). Occasional clasts of anorthositic gabbro are likely derived from the underlying Bird River sill and

suggest that uplift and erosion of the underlying rocks, possibly related to extensional faulting, may be the locus for deposition of the lower diverse arc assemblage. The upper part of the sequence consists of turbidites, fragmental volcanic rocks reworked by mass flows, and aphyric, quartz-amygdaloidal andesite (Gilbert 2007).

Younging reversals (graded beds, scour surfaces, flame and rip-up structures) observed in sediments define localized folding in the diverse arc assemblage. An east-trending anticlinal fold structure occurs near the junction of Provincial Road 314 and 315 (Gilbert 2006; Duguet et al. 2007). The diverse arc assemblage is inferred to be in fault contact with the underlying MORB-type basalt to the north. The upper (southern) contact with the overlying Peterson Creek formation is interpreted as being either conformable or disconformable (Gilbert 2007).

#### 2.3.1.6 Peterson Creek Formation

The predominantly calc-alkaline felsic volcanic and associated volcanoclastic rocks that characterize the Peterson Creek Formation extend east from the shore of Lac du Bonnet across the entire length of the belt to Bird Lake and have been dated at  $2731.1 \pm 1$  Ma (Duguet et al. 2006). The main lithologies are aphyric to quartz- and feldspar-phyric rhyolitic and dacitic flows that grade into autoclastic breccia facies (Gilbert 2007). Duguet (2006) subdivided the Peterson Creek Formation into 2 members based on mapping between the Maskwa-Dumbarton mines and Provincial Road 314. The lower member consists of massive volcanic flows (basalt-dacite-rhyolite) interlayered with pyroclastic deposits ranging from breccia with decimeter-sized clasts to ash-flow tuff. The upper member is composed of thinly-bedded aphyric to quartz-phyric rhyolite and

tuff overlain by massive to crudely layered felsic lapilli tuff and volcanic sandstone (Duguet et al. 2006).

The absence of younging indicators in the Peterson Creek Formation creates difficulty in interpreting detailed stratigraphic relationships between various lithologies. The repetition of various marker units across strike, however, suggests that some degree of folding (Duguet et al. 2006) and/or fault stacking (Gilbert 2007) has occurred throughout the Peterson Creek Formation. The southern limit of the Peterson Creek Formation is in fault contact with the Booster Lake Formation

#### 2.3.1.7 Booster Lake Formation

The east-west trending, fault-bounded Booster Lake Formation is a dominantly greywacke-mudstone turbidite sequence (Cerny et al. 1981, Gilbert 2005) that extends for approximately 44 km and marks the structural boundary between the north and south panels of the Bird River greenstone belt (Gilbert 2006, 2007). The Booster Lake Formation displays many features of a classic Bouma sequence, and primary features such as graded beds, rip-up clasts, flame, and scour structures are abundant and provide reliable top determinations throughout (Cerny et al. 1981; Gilbert 2005). In the eastern part of the sequence, the thinly bedded cyclical turbidites of mainly intermediate composition, indicate a more distal depositional environment. In the west, thicker beds of interlayered coarse-grained felsic wacke, siltstone, and pebble to cobble conglomerate are more indicative of proximal deposition (Cerny et al. 1981, Gilbert 2007). Outcrops of iron formation occur in the west associated with conglomerate (Cerny et al. 1981).

Gilbert (2005) identified a series of early isoclinal folds in the Booster Lake Formation that are persistent in the central and western parts of the belt. The axial traces of the folds are oblique to the belt-scale faults that mark the margins of the formation, and no evidence of similar folding is manifest across the faults, leading to the interpretation of an isoclinal folding event prior to faulting and the structural juxtaposition of the Booster Lake formation to its current tectonostratigraphic position (Gilbert 2005, 2007). The maximum age of the Booster Lake Formation is best constrained by the youngest detrital zircon, which yielded a subconcordant age of  $2712 \pm 17$  Ma (Gilbert 2006).

#### 2.3.1.8 Flanders Lake Formation

The Flanders Lake Formation occurs in the northeastern corner of the Bird River greenstone belt, and delineates a major west to northwest trending anticline that refolds earlier fold structures identified in the Booster Lake Formation (Gilbert 2007). The fluvial-alluvial deposits of the Flanders Lake formation consist of cross-bedded arkosic to pebbly sandstone, polymictic conglomerate, and their gneissic equivalents. The regional map pattern shows an angular relationship between the Flanders Lake Formation and the volcanic and sedimentary rocks of the Peterson Creek, Bernic Lake, and Booster Lake Formations, suggesting an unconformable and/or faulted contact. Detrital zircon analyses yielded a maximum age of deposition of  $2697 \pm 18$  Ma (Gilbert 2006).

### 2.3.2 Intrusive rocks

The Bird River sill is an east-west trending, south-facing, layered mafic-ultramafic intrusion emplaced into the MORB-type basalt in the north panel of the Bird River greenstone belt. The Bird River sill consists of a basal ultramafic series, a transitional series, and an upper mafic series (Theyer 1990; Theyer et al. 2001; Peck et al. 2002). The ultramafic series is composed largely of serpentinized peridotite with lesser dunite and pyroxenite. Chromitite layering occurs in abundance in a 60 m horizon towards the top of the ultramafic series; individual chromite layers range from 3-30 cm in thickness (Mealin 2005). The transitional series contains upper and lower peridotite zones separated by gabbro, and the mafic series consists of differentiated gabbroic zones (Mealin 2006). The sill is overlain by the diverse arc assemblage; the presence of cobbles of anorthositic gabbro derived from the sill in a polymictic conglomerate suggests that the sill was uplifted and subaerially exposed prior to deposition of the diverse arc assemblage (Gilbert 2007). Wang (1993) conducted U-Pb analyses on the Bird River sill and reported an age of  $2744.7 \pm 5.2$  Ma. This date also provides a minimum age for volcanism of MORB-type basalt into which the sill was emplaced. The Bird River sill was historically interpreted to be partially dismembered by extensive normal faulting along northwest trending structures. Recent studies (Mealin 2006, 2008) have interpreted the sill as representing a series of intrusions which have, in part, interacted with one another during emplacement. Medium- to coarse-grained equigranular to subophitic gabbroic intrusions occur throughout the basalt in the northern panel. Their genetic relationship to the Bird River sill is unknown.

The Birse Lake pluton intrudes the MORB-type basalt in the south panel between Bernic Lake and the Winnipeg River. It is a medium- to coarse-grained composite intrusion with compositions ranging from gabbro to granodiorite (Trueman 1980; Cerny et al. 1981). In map pattern, the surficial expression of the Birse Lake pluton shows large-scale (sinistral) asymmetry. Zones of cataclasis and protomylonite occur throughout the Birse Lake pluton and are especially pronounced towards the margins (Kremer 2006).

A gabbroic to dioritic body dubbed the Tanco gabbro occurs northwest of Bernic Lake and is the host rock for the Tanco pegmatite. The Tanco gabbro is medium- to coarse-grained and equigranular. The margins of the gabbro show strong deformation features, including a well-defined, east-west trending, steeply dipping foliation and local narrow, high strain zones. Several smaller gabbro occurrences have been noted on surface and intersected by drill core in the vicinity of Bernic Lake.

The Lac du Bonnet Batholith is emplaced along the crustal-scale fault marking the boundary between the Bird River greenstone belt and the Winnipeg River batholithic belt. It is a polyphase intrusion consisting of 5 major phases: 1) gneissic hornblende-biotite tonalite; 2) gneissic porphyritic hornblende-biotite granodiorite, 3) leucogranite, 4) equigranular to porphyroblastic biotite, and 5) porphyroblastic biotite granodiorite (Cerny et al. 1987). Boundaries with the surrounding rocks are sharp with respect to the Bird River greenstone belt and gradational with respect to the Winnipeg River batholithic belt (Cerny et al. 1981). U-Pb analyses yielded an age of  $2660 \pm 3$  Ma (Wang, 1993).

The Marijane Lake pluton is emplaced in the northeastern portion of the belt in the nose of a map-scale fold structure. Duguet (2005, 2006) has interpreted the intrusion to be syn-deformational (regional  $G_3$ ).

Pegmatitic granites and associated pegmatites occur throughout the Bird River greenstone belt and are located along major formation-bounding shear zones. In total, nine mineralogically and geochemically distinct pegmatite groups have been identified and characterized (Cerny et al., 1981).

## CHAPTER 3

### Geology and Structure of the Bernic Lake Area

#### 3.1 Introduction

Bernic Lake occurs roughly in the centre of the Bird River greenstone belt, northwest of the Birse Lake granodiorite (Figure 3). This thesis is focused mainly on a fault-bounded section of the Bernic Lake Formation in the vicinity of the Tanco mine, between southern panel MORB-type basalt (south) and the Booster Lake Formation (north). The map area comprises part of the ‘southern structural panel’ as defined by Gilbert (2007). In total, an area of approximately 40 km<sup>2</sup> was mapped: the northern limit is the fault bounded contact between the Bernic Lake Formation and younger clastic sedimentary rocks of the Booster Lake Formation, the southern limit is the Birse Lake granodiorite, the western limit is the western extent of the Tanco gabbro, and the eastern limit is located approximately 1 km east of Bernic Lake (map in back pocket). The area mapped covers the known occurrences (both surface and subsurface) of the Bernic Lake pegmatite group (Cerny et al. 1981).

Based on mapping by Kremer (2005) and Kremer and Lin (2006) and recent geochemistry (Gilbert 2006), two distinct volcanic packages are present around Bernic Lake. To the south, a previously unrecognized MORB-type sequence is attributed to the southern panel MORB-type basalt. To the north, a folded sequence of continental arc-type volcanic (basalt-dacite) and volcanoclastic rocks comprise part of the Bernic Lake Formation. These two sequences are separated along the northern shore of Bernic Lake by a belt-scale shear zone, herein termed the North Bernic Lake Shear Zone (NBLSZ). A

fault contact also exists north of the Bernic Lake Formation where it is thrust over the Booster Lake Formation. This contact is not exposed in the map area, however, a strong east-west lineament is visible in ortho-rectified air photos, and the strain gradient is observed in outcrop in both the Bernic Lake and Booster Lake Formations, increases towards the contact.

## **3.2 Geology of the Bernic Lake Area**

### **3.2.1 Southern panel MORB-type basalt**

Southern panel MORB-type basalt occurs along the southern shore of Bernic Lake and is composed primarily of east-west trending, pillowed basalt flows and lesser massive basalt flows (generally < 20% of the volcanic pile) with MORB-like back-arc geochemical signatures (Gilbert 2006). Pillows weather dark grey to green, are closely packed with thin to medium selvages averaging less than 1 cm in thickness and contain minor amount of interpillow hyaloclastite (Figure 3a). Pillows are generally uniform in size, ranging between 0.8 – 1.2 metres and show a systematic increase in strain and flattening approaching the NBLSZ. Flows are aphyric to feldspar-phyric (with 15% euhedral phenocrysts 0.3 – 0.8 cm), generally non-amygdaloidal and are variably recrystallized to a coarse-grained intergranular textured aggregate of hornblende-plagioclase gneiss. Recrystallization is particularly evident southeast of Bernic Lake, where in a series of outcrops, the presence of relict pillow selvages is the only feature that allows this unit to be identified (Figure 3b). The effects of alteration, deformation and recrystallization, combined with poor outcrop exposure limits the ability to systematically map individual flows. A thin unit (approximately 10 metres thick) of bedded mafic to

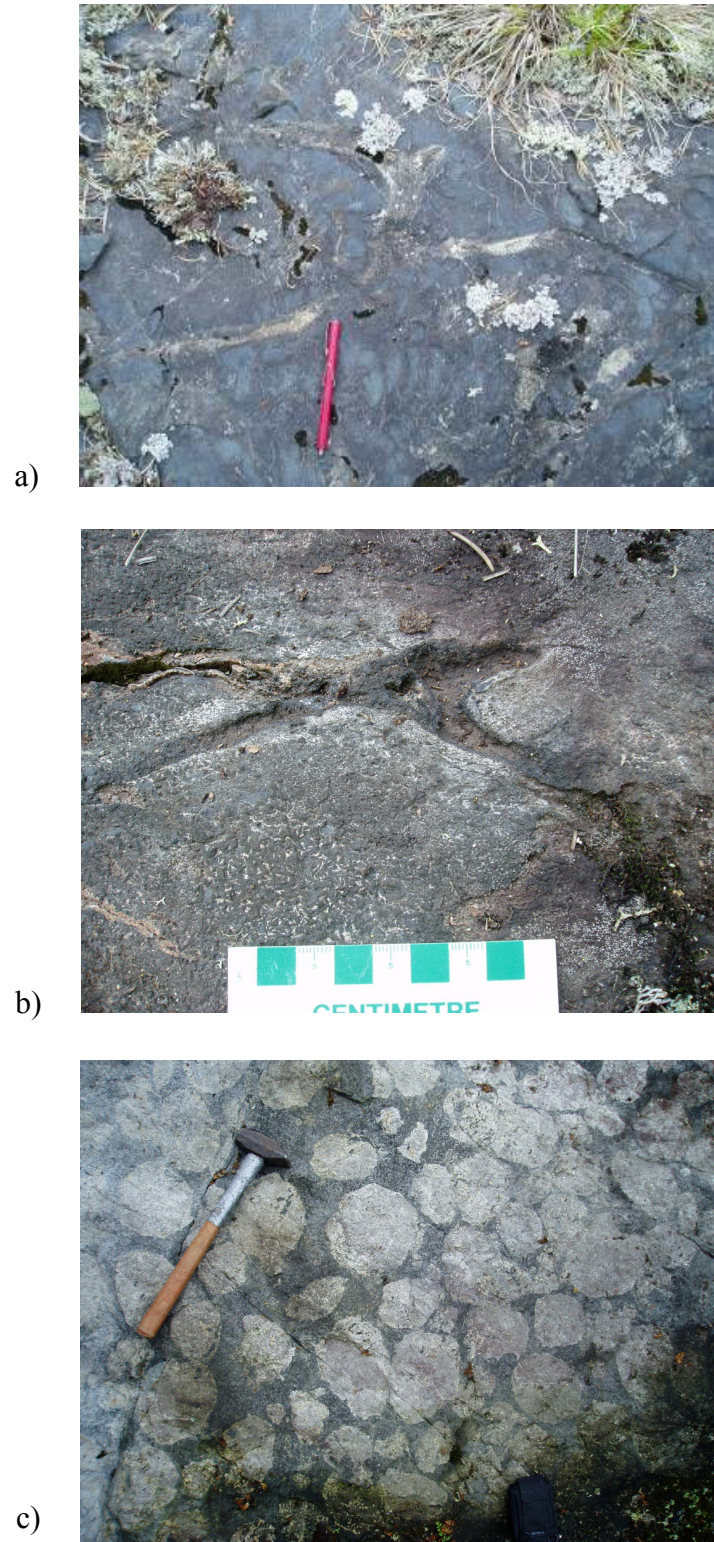


**Figure 3.** Outcrop photographs of the south panel MORB-type basalt, southern shore of Bernic Lake. a) aphyric pillowed flow, b) strongly recrystallized pillowed flow with relict selvage, c) plagioclase glomeroporphyritic gabbro dyke.

intermediate tuff is exposed in places on the southwestern shore of Bernic Lake. Though convincing younging criteria are sparse throughout southern panel MORB-type basalt, where observed tops are consistently to the north.

The iron formation reported in the southern panel MORB-type basalt (see Section 2.4.1.2) elsewhere in the belt (Gilbert 2006, 2007) was not observed in the map area. However, a strong magnetic anomaly is apparent on geophysical surveys immediately south of the map area which indicates the presence of un-exposed iron formation in the vicinity of Bernic Lake. Furthermore, an anomalous compass deviation was noticed in the field south of the southern limit of mapping, immediately west of the Birse Lake granodiorite.

Dykes and sills of glomeroporphyritic gabbro (5 – 10 m thick) with up to 80% feldspar glomerocrysts ranging in size from 5-20 cm intrude the basalt southwest of Bernic Lake (Figure 3c). Owing to the presence of glomeroporphyritic flows elsewhere in the sequence (Gilbert 2005), these are interpreted to form part of a suite of syn-volcanic intrusions.

### **3.2.2 Bernic Lake Formation**

Volcanic and sedimentary rocks of the Bernic Lake Formation extend from the NBLSZ northward to the Booster Lake Formation. Blue-grey to green weathering pillow basalt forms the predominant rock type of the Bernic Lake Formation in the area. Basalt is aphyric and typically contains 5 – 20% quartz-filled amygdales, locally up to 3 cm in diameter. Pillow selvages are generally thick (1 cm) with varying but minor amount of altered interpillow material. Hydrothermal quartz-epidote alteration is prevalent in basalt,

and has resulted in the formation of epidosite nodules in pillow cores and/or zones of intense silicification (Figure 4a). Preservation of primary features in basalt is poor owing to the effects of strong alteration and deformation (Figure 4b).

Distinctive units of quartz- and feldspar-phyric dacite are interleaved with basalt. Massive dacite is well exposed in outcrop, weathers pale grey-blue, and contains 20-30% evenly spaced euhedral quartz and feldspar phenocrysts that range from 2 to 6 mm. Monolithic fragmental dacite, which is localized towards the top of massive dacite units, contains 60-80% clasts with aspect ratios averaging 5:1. Dacite forms discontinuous lenses in the volcanic pile ranging from 0.5 to >5 km in strike length. Where contacts between dacite and basalt are observed, they are sharp and straight with little to no evidence of significant deformation. Dacite and basalt are therefore interpreted to form part of a conformable sequence.

Heterolithic volcanic breccia representing reworking of existing volcanic rocks is locally intercalated with the volcanic rocks. The breccia is clast or matrix supported. In either case, the majority of clasts (> 80%) are of felsic to intermediate composition (dacitic), subangular to rounded, range in size from 2 to 20 cm and are flattened parallel to the dominant  $S_2$  foliation. The remaining 20% of clasts are mafic volcanic derived from basalt (Figure 4c). These deposits are commonly massive in individual outcrops, although exposures with crude to moderately well-developed bedding exist northeast of Bernic Lake (Figure 4d). The breccia cannot be traced continuously along strike owing to poor exposure; however, the occurrence of equivalent rocks in isolated outcrops at roughly the same stratigraphic level supports some degree of lateral continuity of this rock type.

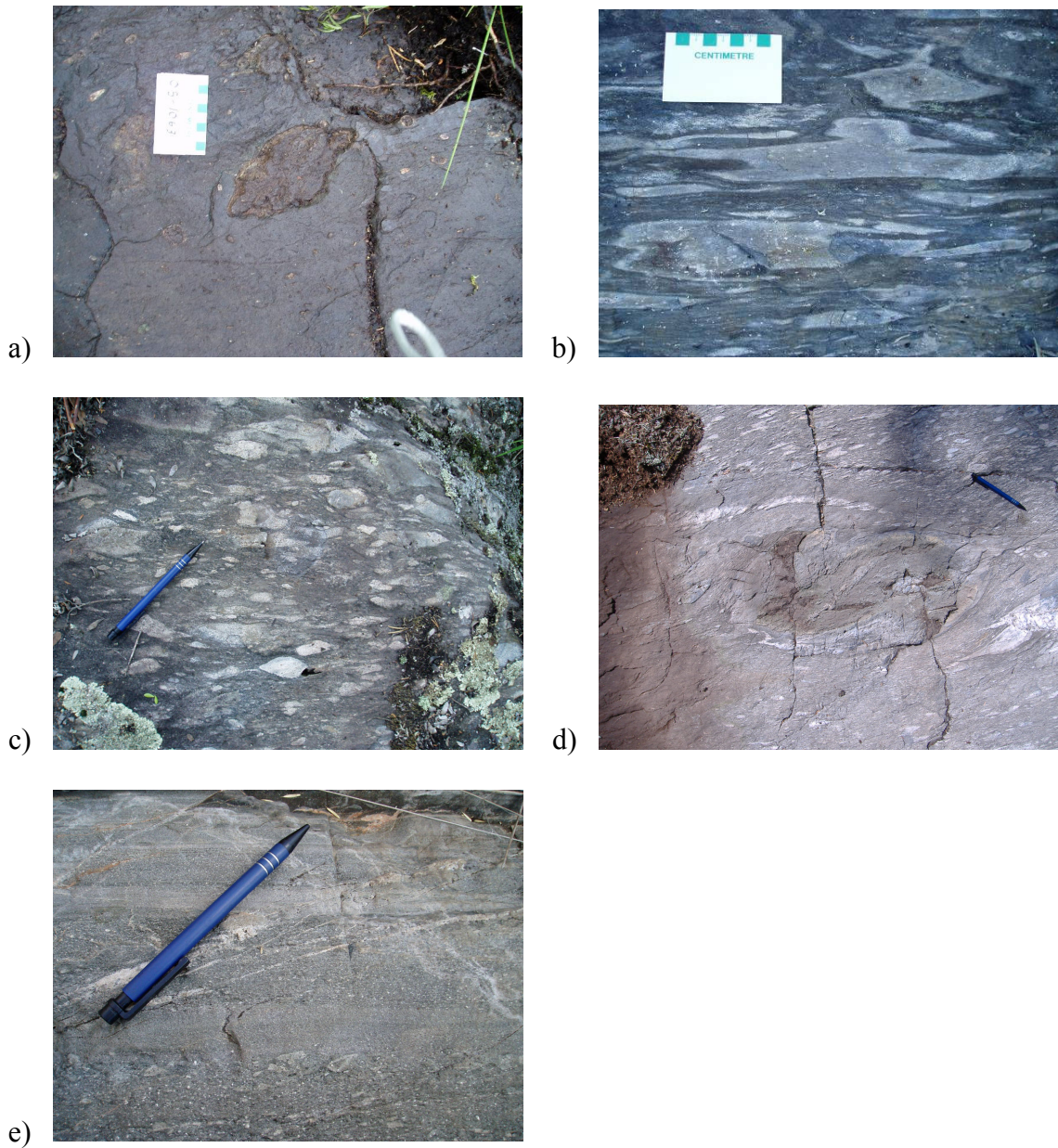


**Figure 4.** Outcrop photographs of the Bernic Lake Formation. a) epidosite ball in basalt, b) strongly altered quartz-feldspar amygdaloidal pillow basalt, c) heterolithic volcanic breccia, d) crude bedding in heterolithic volcanic breccia (note asymmetric dextral tails on large basalt clast in centre of image), e) bedded intermediate to mafic volcanic sandstone with minor pebble conglomerate.

Mafic to intermediate volcanic sandstone with lesser pebble conglomerate is well exposed at the base of hydroelectric poles along the powerline east of the Tanco mine (Figure 4e). The volcanic sandstone is fine- to medium-grained and well-bedded. Bed thickness ranges from 3 to 30 cm and normal graded bedding is occasionally useful for top determinations.

Younging criteria are not abundant in the Bernic Lake Formation. Along the southern margin of the formation near the NBLSZ, two south facing tops were identified. Well-defined, south-facing, normal graded bedding in volcanic sandstone was observed south of the Tanco mine near the western edge of the map area and south-facing pillows are found east of Bernic Lake, in pillow basalt that hosts the Buck pegmatite. Outcrops exhibiting south tops are limited to the area immediately north (< 200 m) of the NBLSZ. All other younging criteria identified in the Bernic Lake Formation are consistent with tops to the north.

### **3.2.3 Booster Lake Formation**

The Booster Lake Formation occurs along the northern margin of the map area. These rocks were not examined in detail for this project, but rather used to define the northern limit of mapping. The Booster Lake Formation consists of fine- to locally medium-grained, well-bedded greywacke-mudstone turbidites. Bedding is generally thin (cm-scale), though m-scale beds of greywacke were observed in one location north of the Tanco mine. Primary features, which include graded bedding, scour and flame structures, are generally well-preserved. Locally, mudstone layers contain up to 60% altered cordierite porphyroblasts.

### **3.2.4 Tanco gabbro**

The Tanco gabbro occupies the northwestern portion of the map area and is approximately 1.5 km x 3 km in size. Through much of its extent it is medium- to coarse-grained, equigranular and homogeneous containing 60% hornblende and 40% plagioclase; however, several outcrops display dramatic textural variations. Both fine-grained and pegmatitic segregations can be found west of the Tanco mine, and towards the southern and western margins, leucocratic phases are common (Figure 5a). No consistent crosscutting relationships exist between mafic and leucocratic phases. In some localities, gabbroic rocks are clearly intruded by granodiorite with irregular contacts, however in adjacent outcrops, xenoliths of leucocratic material occur as rafts in gabbroic rocks (Figure 5b). These conflicting relationships suggest that some degree of magma mingling occurred. East of the Tanco mine, fingers of gabbro 20-50 m thick extend into mafic volcanic rocks of the Bernic Lake Formation. Narrow, discrete high strain zones occur locally throughout the Tanco gabbro and are especially prevalent along the margins of the intrusion.

### **3.2.5 Birse Lake granodiorite**

The Birse Lake granodiorite is a medium-grained, quartz- and feldspar-phyric intrusion extending across the entire southern boundary of the map area. Contacts with the country mafic volcanic rocks (Lamprey Falls Formation) are generally not exposed, but can be limited to a few meters where outcrops are better exposed. Dykes emanating from the Birse Lake granodiorite bear striking petrographic similarities to dacite in the Bernic Lake Formation. The northern contact is moderately mylonitized.



**Figure 5.** Outcrop photographs of the Tanco gabbro. a) late-stage pegmatitic phase, b) inclusions of gabbro in leucogabbro/quartz diorite.

### **3.2.6 Bernic Lake pegmatite group**

The Bernic Lake pegmatite group belongs to the LCT (Li, Ce, Ta) family and is classified as a highly fractionated, complex type, petalite sub-type (Vanstone 2002), enriched in rare-elements, Li, Rb, Cs, Be, Sn, Ta, Nb, B, P, F, Zr and Hf (Cerny et al. 1981). Internal zonation and pronounced alteration haloes are common, particularly in the larger pegmatites of the group (Lenton 1979; Cerny et al. 1981; Morgan and London 1987). The Bernic Lake pegmatite group is poorly exposed in the area, and has been largely defined on the basis of diamond drill intersections. With the exception of the Tanco pegmatite, which occurs in the northwestern corner of Bernic Lake, the majority of occurrences are located east of the lake and intrude both the south panel MORB-type basalt and the Bernic Lake Formation. All the pegmatites are localized around the NBSZ (Figure 6). Where exposed, pegmatites have a variety of attitudes with dips ranging from subhorizontal (e.g. Tanco) to subvertical. Contacts with the host rocks are always sharp. In some cases contacts are straight and pegmatites are tabular, whereas in other cases contacts are highly irregular and indicative of boudinage and folding. Aside from the Tanco pegmatite, which is very well constrained by extensive diamond drilling, the 3-dimensional shapes of the various pegmatites in the group are not well known.

### **3.3 Structural Geology of the Bernic Lake Area**

On the basis of overprinting relationships, five generations of deformation structures will be described in turn in the following sections.  $G_1$  and  $G_2$  show purely ductile features,  $G_3$  and  $G_4$  are locally manifest and show evidence of both ductile and brittle deformation, and the final event involves a late, purely brittle overprint.

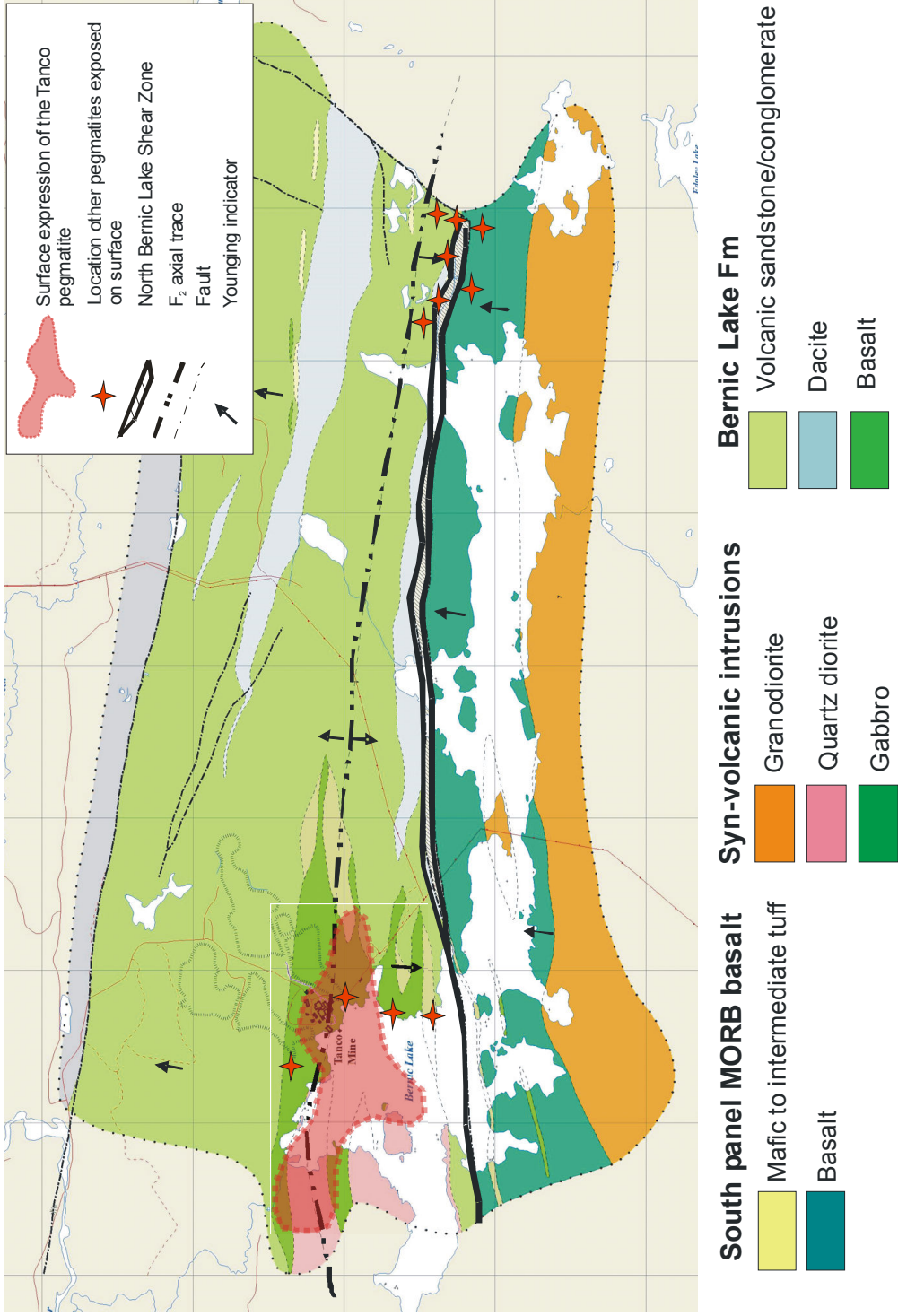


**Figure 6.** Geology of the Bernic Lake area showing the approximate location of pegmatites in the Bernic Lake pegmatite group.

### 3.3.1 G<sub>1</sub> structures

Structures attributed to G<sub>1</sub> deformation are sparse and are only found in low-strain zones, such as in the hinges of meso-scale F<sub>2</sub> folds. At one location northeast of Bernic Lake, an early isoclinal fold (F<sub>1</sub>) is refolded by an upright F<sub>2</sub> fold (Figure 7). Other examples include rare, poorly developed S<sub>1</sub> foliation observed around the nose of F<sub>2</sub> folds. On the limbs of these F<sub>2</sub> folds, the S<sub>1</sub> fabric is completely transposed and therefore indistinguishable from the overprinting, penetrative S<sub>2</sub> foliation.

Owing to its near obliteration by subsequent deformation structures, the nature and tectonic significance of G<sub>1</sub> deformation are very poorly constrained around Bernic Lake. This event is potentially related to early isoclinal folding identified in the Booster Lake Formation (Gilbert 2005) and/or thrusting that resulted in the juxtaposition of the south panel MORB-type basalt against the Bernic Lake Formation along the north Bernic Lake shear zone (Duguet 2007). However, the truncation of F<sub>1</sub> fold axes in the Booster Lake Formation by formation-bounding shear zones, suggests that their development occurred prior to shearing (Gilbert 2005, 2007). This interpretation is also preferred for F<sub>1</sub> folds in the Bernic Lake area.

### 3.3.2 G<sub>2</sub> structures

Structures formed during G<sub>2</sub> deformation are the most prominent in the Bernic Lake area and affects all lithologies to varying degrees. The resulting structures include a penetrative flattening foliation (S<sub>2</sub>) with associated stretching lineation (L<sub>2</sub>), meso- to macro-scale folds (F<sub>2</sub>) and initiation of the north Bernic Lake shear zone (NBLSZ).



**Figure 7.** Rarely preserved isoclinal  $F_1$  fold refolded by upright  $F_2$  fold.

The predominant structural element associated with  $G_2$  deformation is a penetrative flattening foliation ( $S_2$ ), defined by moderate to intensely stretched and flattened primary features (e.g., pillows and clasts), as well as a closely-spaced layer-subparallel foliation defined by the preferred alignment of hornblende and biotite, which is locally accentuated by narrow quartz veinlets that parallel the foliation planes.  $S_2$  is present in all lithologies in the map area with the exception of late intrusive rocks (pegmatites). The  $S_2$  foliation strikes east to east-southeast and dips steeply to the south. However, along the northern margin of the Birse Lake pluton,  $S_2$  dips to the north. A locally well developed down-dip stretching and lineation ( $L_2$ ) is present on  $S_2$  foliation planes. The  $L_2$  stretching lineation is most readily observed in well-exposed outcrops of heterolithic volcanic breccia and fragmental dacite, where stretched clasts plunge moderately to steeply southwest (Figure 8). A coincident intersection lineation and mineral lineation defined by elongate hornblende crystals in altered basalt parallels the  $L_2$  stretching lineation. Hornblende crystals do not exhibit evidence of stretching or boudinage that might suggest growth during deformation. It is possible that rather than having formed in direct response to  $G_2$  strain, the observed mineral alignment is a result of growth anisotropy preferentially along the intersection lineation during peak amphibolite prograde metamorphism. This is supported by Duguet et al. (2005, 2006) who found that the  $S_2$  foliation is overgrown by garnet porphyroblasts in mafic volcanic rocks of the Bernic Lake Formation. In some instances, garnets show minor rotation (asymmetric strain shadows, slightly rotated inclusion trails) consistent with the  $G_2$  kinematic frame, however, in many cases they appear to post-date shearing, and thus indicate that peak metamorphism outlasted, or post-dated,  $G_2$  deformation.

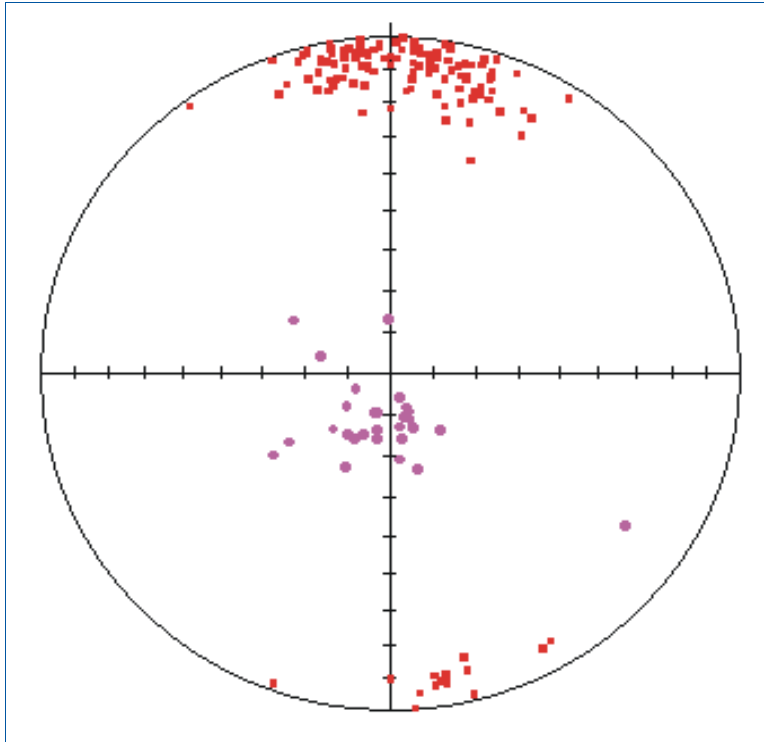


**Figure 8.** Lower hemisphere equal area plot showing the orientations of G<sub>2</sub> fabric elements in the Bernic Lake area. Red dots (n = 127) represent poles to S<sub>2</sub> foliation planes, Purple dots (n = 29) represent L<sub>2</sub> stretching and mineral lineations.

The  $S_2$  foliation is axial planar to cm- to m-scale upright folds ( $F_2$ ) observed in outcrop in the Bernic Lake area.  $F_2$  folds are tight to isoclinal, have sub-vertical axial planes and plunge moderately to steeply southwest, subparallel to  $L_2$ . On the basis of rare younging reversals in the Bernic Lake Formation, a large-scale  $F_2$  fold structure is inferred, the axial trace of which trends in an east-west direction immediately north of Bernic Lake. In a few outcrops along its axial trace, symmetric folds are developed. Rare parasitic folds on the northern limb exhibit z-asymmetry; the southern limb is attenuated by the NBLSZ and no parasitic folds were observed. The inferred axial trace of the large  $F_2$  fold also crosses the Tanco pegmatite. Discrete folding in the Tanco pegmatite is observed at underground exposures of the aplitic albite zone (Figure 9), however the Tanco pegmatite clearly crosscuts the  $S_2$  axial planar foliation, precluding  $G_2$  deformation as a cause. The folds likely formed as primary features during crystallization.

Movement along the NBLSZ, a locus for intense shear deformation that runs along the northern shore of Bernic Lake and separates the Bernic Lake Formation from the south panel MORB-type basalt, is also attributed to  $G_2$  deformation. The NBLSZ, which is 20 – 100 m thick in the map area, is characterized by a marked increase in strain relative to the surrounding country rocks and complete obliteration of primary structures. A change in the orientation of the NBLSZ from east-northeast to east-southeast (dip is subvertical in both cases) occurs near the north-central bay in Bernic Lake. Stretching and ridge-in-groove lineations along shear foliation planes are down-dip and parallel to  $L_2$ . Kinematic indicators, including  $\sigma$ -porphyroclasts and asymmetric boudinage of quartzofeldspathic veins, indicate south-side-up sense of displacement in the vertical

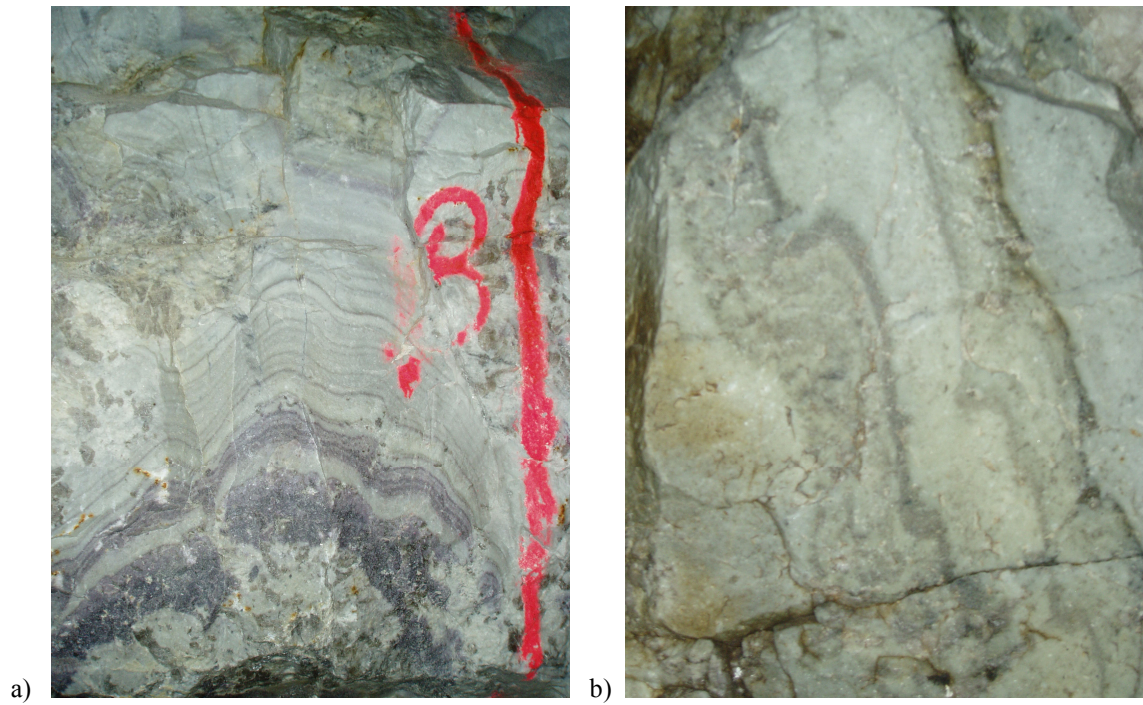


**Figure 9.** Upright folds in the albitic aplite zone, underground at the Tanco mine. Although the style and orientation of these folds are consistent with  $F_2$  folds identified on surface in supracrustal rocks of the Bernic Lake formation, they cannot be confidently linked to the same generation of deformation.

plane (Figure 10a). Where the NBLSZ trends east-northeast, kinematic indicators in the horizontal plane are absent. In the eastern half of the map area, where the NBLSZ trends east-southeast, rare drag folds, shear bands, and asymmetric boudins are consistent with a component of dextral shear in the horizontal plane (Figure 10b). A shear contact is also inferred between the Bernic Lake and Booster Lake Formations. Although a pronounced lineament exists, the contact is not exposed in the map area. However, a strain gradient is present in basalt of the Bernic Lake Formation adjacent to the contact. Furthermore, the stratigraphic position of the younger turbidites north of the older volcanics is consistent with the relationships that are observed across the NBLSZ and with a dominantly south-side-up sense of shear.

$G_2$  deformation is interpreted to record N-S directed shortening at amphibolite grade, which resulted in the formation of  $S_2$ ,  $L_2$ , and  $F_2$  structures. Continued compression led to increased localized strain and south-side-up shear along the formation-bounding shear zones, which in the case of the NBLSZ, occurs along the attenuated limb of a macro-scale  $F_2$  fold.

### **3.3.3 $G_3$ structures**

A spaced cleavage overprints the penetrative  $S_2$  foliation and is attributed to  $G_3$  deformation. The  $S_3$  cleavage is only locally developed and is more prominent towards the eastern end of Bernic Lake in mafic volcanic rocks.  $S_3$  trends northeast to east-northeast, is steeply-dipping, and is consistently oriented 10-15° counterclockwise with respect to  $S_2$ . This is most obvious in pillow basalt where the  $S_3$  cleavage is oblique to the

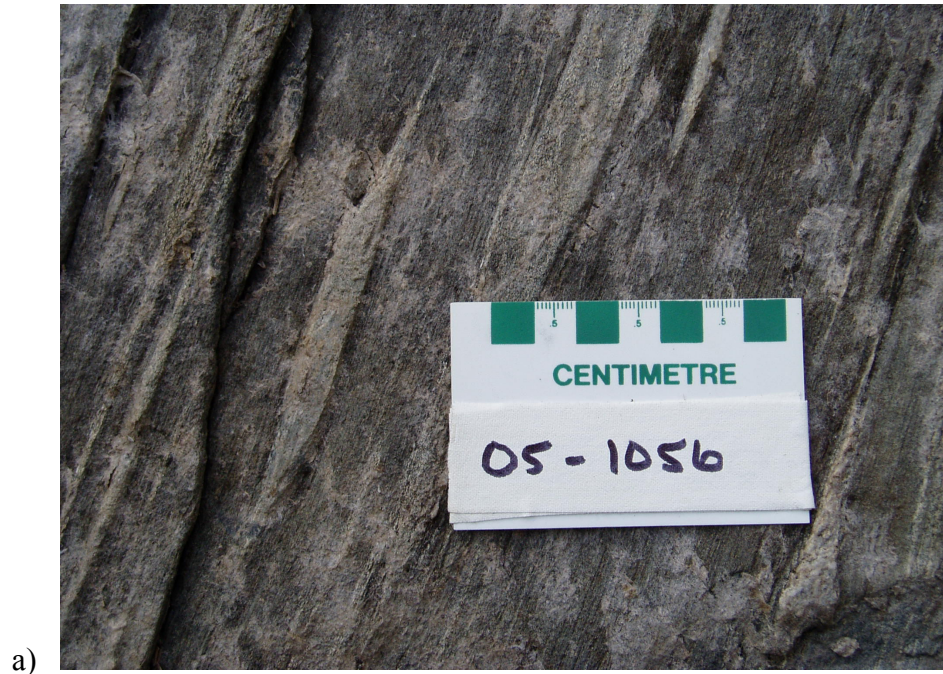


**Figure 10.** Outcrop photographs of kinematic indicators in the North Bernic Lake shear zone. a)  $\sigma$ -porphyroclast showing south-side-up movement (south is to the left of the photograph), 2) z-asymmetric drag fold indicating a local component of dextral shear east of Bernic Lake.

long axis of stretched pillows. The cleavage is locally accentuated by the intrusion of fine-grained gabbroic and feldspathic aplite dykes along cleavage planes (Figure 11).

Although fabric elements in the NBLSZ are also locally overprinted by  $S_3$  indicating the cessation of shearing prior to the onset of  $G_3$  deformation, east of Bernic Lake, strong evidence for reactivation of the NBLSZ during  $G_3$  deformation exists. Narrow east-west trending, subvertical, dextral ductile-brittle shear zones, where observed in association with  $S_3$ , show S-C type relationships. Cleavage planes show minor clockwise rotation into the shear planes (defined by  $S_2$  foliation planes). Since there is no evidence for significant deformation post-dating  $G_3$ , this indicates that the reactivation of  $S_2$  fabric elements is synchronous with the development of  $S_3$ . Because shear fabrics associated with  $G_3$  deformation are subparallel to and reactivate  $S_{0/2}$  structures (in particular along the NBLSZ) with similar kinematics, differentiating between the two generations is difficult. It is possible that the dextral shear fabrics observed along the NBLSZ in the eastern half of the map area resulted, either in part or entirely, from reactivation during  $G_3$ . The orientation of  $G_3$  structures indicates NNW-SSE directed shortening during  $G_3$  deformation.

### **3.3.4 $G_4$ structures**

Two prominent fracture sets (that host the Tanco pegmatite) within the Tanco gabbro are inconsistent with data from and are overprinted by late, brittle deformation (see Section 3.3.5). The fractures strike WSW and ESE, and dip shallowly to the south and northwest respectively. The acute angle between the two fractures is approximately  $45^\circ$ . At numerous exposures underground at the Tanco mine, the fractures display



**Figure 11.** Outcrop photograph showing oblique relationship between S2 (parallel to the stretching axis in the pillows) and S3 (parallel to fine-grained gabbroic dyke) in the Bernic Lake Formation.

mutually overprinting relationships, which is evidence that they are temporally related (Figure 12). Furthermore, the two fracture sets have opposing senses of displacement (normal slip along one fracture plane, reverse slip along the second fracture plane). The orientations of the fractures, their mutually crosscutting relationships, and their antithetic senses of slip with respect to one another (Figure 12) indicate that they form a conjugate set. In conjugate fracture sets, the line of intersection between the two fracture planes corresponds to the intermediate stress vector ( $\sigma_2$ ). The maximum ( $\sigma_1$ ) and minimum ( $\sigma_3$ ) stress vectors occur on a plane perpendicular to  $\sigma_2$ , and respectively bisect the acute and obtuse angles between the two fracture planes. Using this principle, simple reconstruction of paleostress directions indicate that the conjugate set formed under NNW-SSE directed, subhorizontal shortening with vertical extension direction (Figure 13).

The inferred principal shortening axes related to  $G_3$  and  $G_4$  structures are parallel to one another. The strong similarities in orientation and kinematics between  $G_3$  and  $G_4$  deformation events suggest that  $G_4$  may be a continuation of  $G_3$  deformation during a single progressive  $D_3$  event. Given the systemic change from ductile to ductile-brittle structures through the course of these events,  $G_{3,4}$  deformation may record the onset of uplift and exhumation of the Bernic Lake Formation, at or near the brittle-ductile transition. Whereas the  $G_2$  structural elements are consistent through all lithologies, the accommodation of  $D_3$  deformation resulted in both  $G_3$  ductile structures in mafic metavolcanic rocks ( $S_3$  cleavage reactivation of the pre-existing NBLSZ) and  $G_4$  brittle structures in gabbro (conjugate fracture set). The response to  $D_3$  strain, therefore, is largely controlled by the competencies of the rocks on which it is subjected.

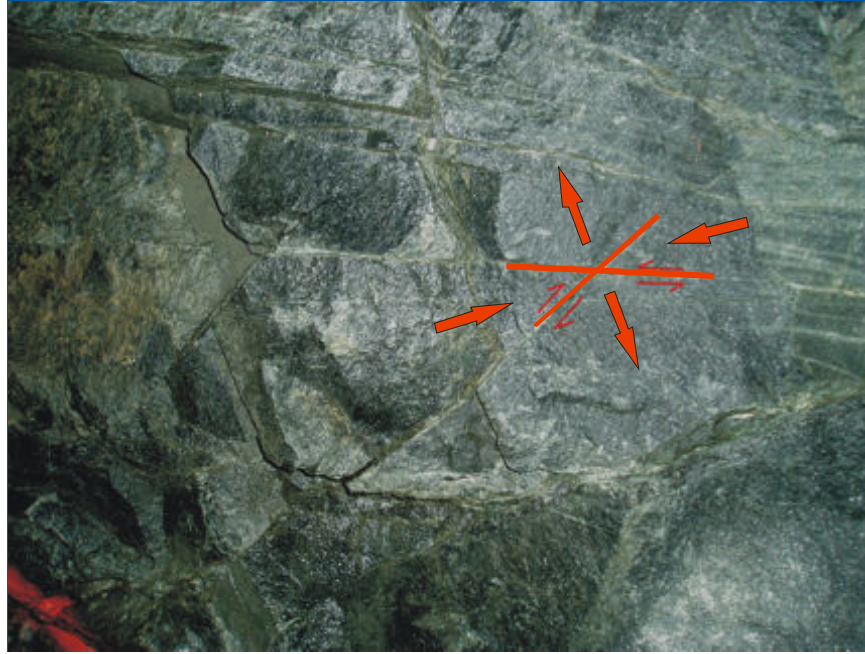


**Figure 12.** Photograph showing the mutually overprinting relationship and opposing senses of slip along conjugate fracture planes in the Tanco mine.

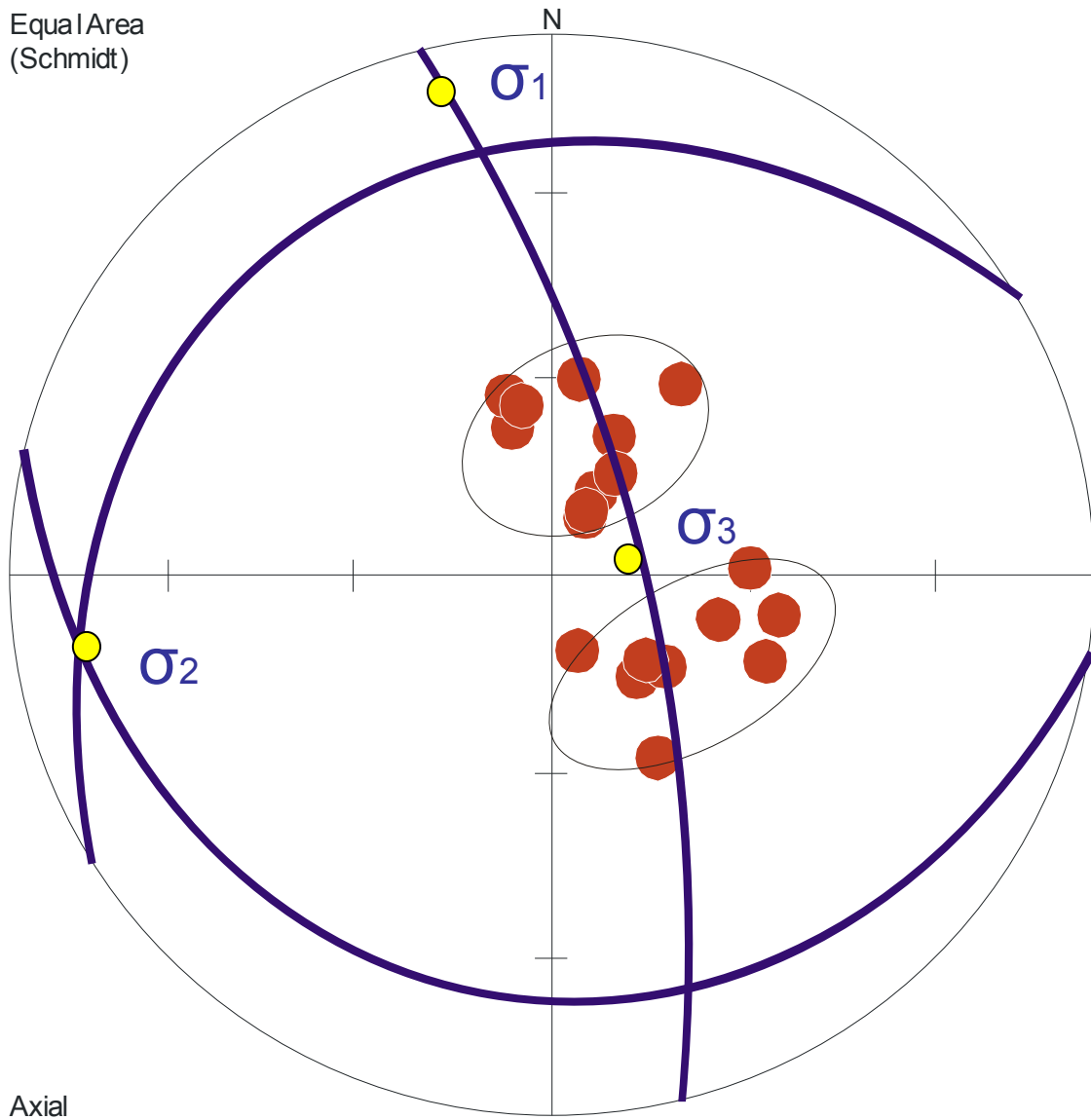


**Figure 13.** Lower hemisphere equal area stereonet showing the orientation of the conjugate fracture set (red dots) along which the Tanco pegmatite intruded. Paleostress reconstructions based on this data indicate the fractures formed as a result of subhorizontal, NNW directed shortening ( $\sigma_1$ ) with subvertical extension ( $\sigma_3$ ).

### **3.3.5 Late, brittle deformation**

Evidence for late brittle fracturing and faulting that overprints all preexisting structures is widespread throughout the map area. Plotted on Figure 14 are data showing the orientations of brittle fractures in the Bernic Lake area. Two dominant orientations are evident: 1) north-south trending, subvertical; and 2) northeast-southwest trending, moderately dipping (Figure 14). Only minor displacements ( $\ll 1$  m) were observed along fracture planes. Strong lineaments consistent with fracture set 1 are clearly visible on aerial photographs. Exposure along these lineaments is poor, but large, scarp-like features exist along their length, possibly representing late, brittle faults. However, no slickenlines or fault-rocks were observed along the scarp-like surfaces and lithological contacts can be traced across them with little or no apparent horizontal displacement. Subvertical fractures have also been observed to crosscut pegmatites in the area, including the Tanco pegmatite (Figure 15), providing a relative constraint on the minimum timing of pegmatite emplacement.

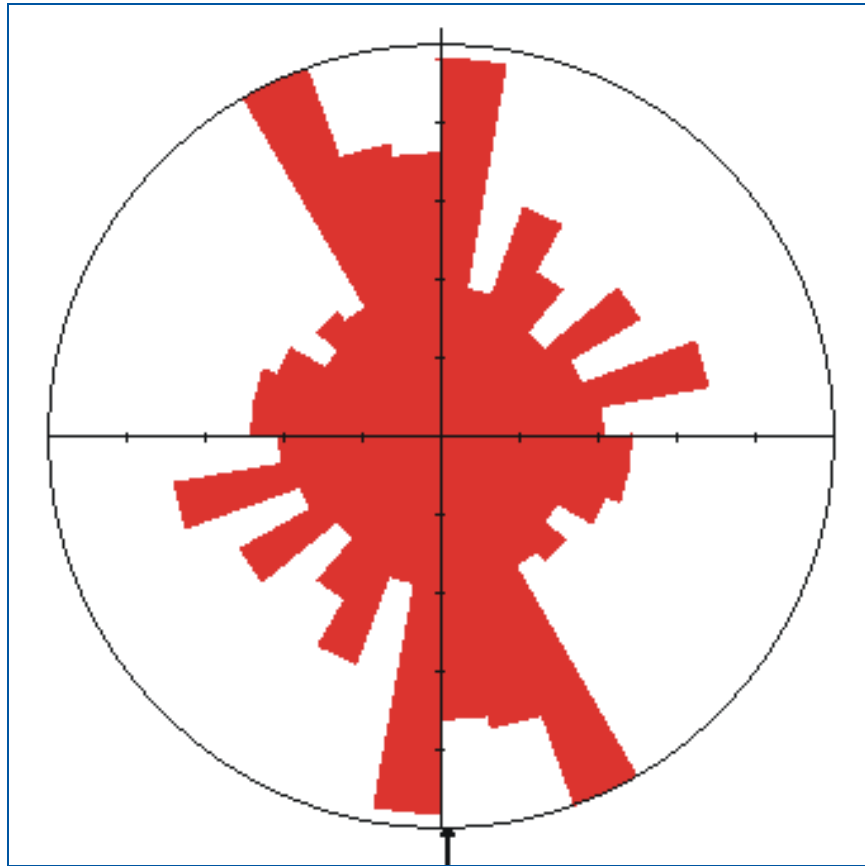


**Figure 14.** Rose diagram showing the orientations of late, post-tectonic fractures in the Bernic Lake area (n = 371).

### **3.4 Relationship of the Bernic Lake Pegmatite Group to Structural Elements**

As a first order observation, all pegmatites in the Bernic Lake pegmatite group that were observed in the field are located in proximity to the NBLSZ, suggesting that this major  $G_2$  structure is an important control on the localization pegmatitic melt. Pegmatites in the Bernic Lake pegmatite group show two distinct styles of emplacement with respect to the deformation structures identified in the Bernic Lake Formation: shear-hosted pegmatites, which occur in highly deformed metavolcanic rocks, and fracture-hosted pegmatites, which occur in gabbro.

The Oompa Loompa pegmatite, which is exposed approximately 500 m east of Bernic Lake, is emplaced within the NBLSZ and crosscuts the pervasive  $G_2$  foliation, suggesting that it post-dates  $G_2$  deformation. Folding and boudinage of the pegmatite, however, indicate that ductile deformation was ongoing during emplacement (Figure 15). Lenton (1979) described down-dip boudinage in the Buck pegmatite, which also occurs east of Bernic Lake. The Oompa Loompa pegmatite is crosscut by a late brittle fault attributed to  $G_5$  deformation (Figure 15), providing a relative minimum constraint on emplacement with respect to deformation events. On the basis of these observations, two possibilities exist: 1) the Oompa Loompa pegmatite was emplaced along the NBLSZ during the final stages of  $G_2$  deformation, or 2) the Oompa Loompa was emplaced during reactivation of NBLSZ during  $G_3$  deformation.

Pegmatites occurring in gabbro (Tanco pegmatite) are emplaced along conjugate fractures interpreted as  $G_4$  structural elements (Figure 16a). The Tanco gabbro contains a well-developed  $G_2$  foliation which is crosscut by the Tanco pegmatite. In addition, the  $G_2$  foliation in large rafts of gabbro encapsulated in the pegmatite has been rotated with

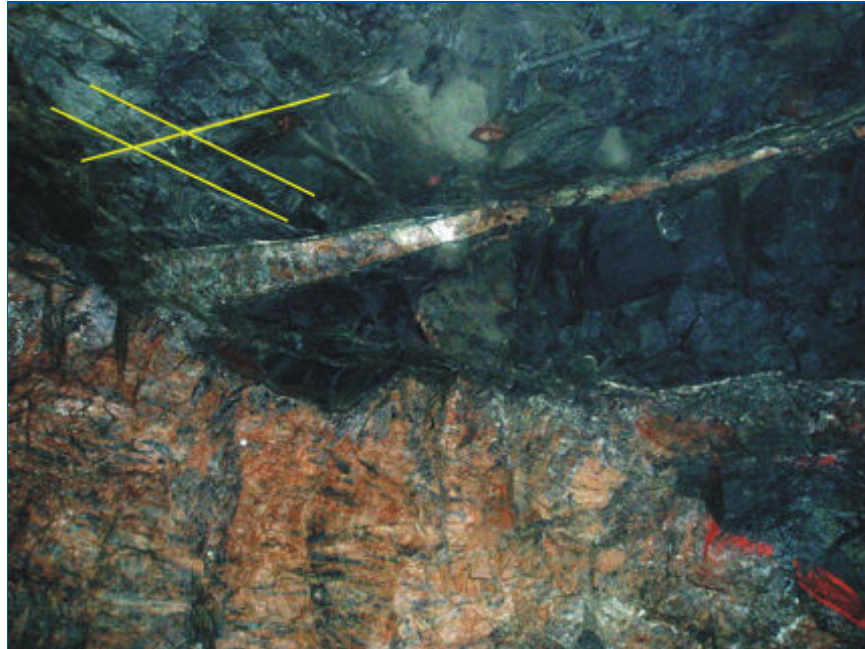


a)



b)

**Figure 15.** Outcrop photographs of the Oompa Loompa pegmatite emplaced within the NBLSZ east of Bernic Lake. a) overview of outcrop showing folding of pegmatite (fold axial trace is sub-parallel to shear foliation in host rocks); b) close up of outcrop showing pegmatite crosscutting S2 shear foliation, incipient boudinage (top right of photo) and late brittle dextral fault).



a)



b)

**Figure 16.** Photos taken underground at the Tanco mine showing the relationship of the Tanco pegmatite to the various generations of fractures. a) Tanco pegmatite emplaced along G4 conjugate fracture set; b) the Tanco pegmatite being crosscut by post tectonic, sub-vertical fractures.

respect to the  $G_2$  foliation in the wall rock. The Tanco pegmatite is crosscut by  $G_5$  brittle fractures in numerous locations (Figure 16b).  $G_3$  structures were not observed around the Tanco pegmatite and its relative timing with respect to  $G_3$  deformation is unknown. These relationships indicate that the Tanco pegmatite postdates  $G_2$  folding and shearing and that it was emplaced during (or after)  $G_4$  conjugate fracture development in the gabbro, but prior to  $G_5$  fracturing.

The preferred interpretation based on the above constraints is that shear-hosted pegmatites were emplaced during  $G_3$  deformation and fracture-hosted pegmatites were emplaced during  $G_4$  deformation. This raises the possibility that two generations of pegmatite could exist within the Bernic Lake pegmatite group: 1) earlier, syn- $G_3$  shear-hosted pegmatites; and 2) later, syn- $G_4$  fracture-hosted pegmatites. However, if  $G_3$  and  $G_4$  structures are contemporaneous (as proposed in Section 3.3.4), then shear-hosted pegmatites east of Bernic Lake and fracture-hosted pegmatites in gabbro are also contemporaneous, and should therefore yield overlapping U-Pb ages.

## **CHAPTER 4**

### **U-Pb Geochronology of the Bernic Lake area**

#### **4.1 Introduction**

Isotopic U-Pb analyses are critical tools in deciphering the geologic history of an area. The analyses can determine absolute ages of rocks that can be used to evaluate their temporal and genetic relationships with respect to one another and with major geological events such as deformation and metamorphism. Geochronological data in the Bernic Lake area is limited. Aside from an age of  $2640 \pm 7$  Ma for the Tanco pegmatite (Baadsgaard and Cerny, 1993), only relative ages based on overprinting relationships inferred from field observations exist in the map area. In order to meet the goals of this project, 5 samples of various lithologies were collected for U-Pb analysis. Descriptions and purposes of each sample, as well as the results of analyses are discussed in the following sections.

#### **4.2 Analytical Techniques**

Samples for this thesis were collected during mapping in the summers of 2005 and 2006. All samples were processed and analyzed at the Jack Satterly Geochronology Laboratory at the University of Toronto. The majority of U-Pb data was gathered from individual zircon and tantalite grain analyses using isotope dilution-thermal ionization mass spectrometry (ID-TIMS) methods. Thermal extraction-thermal ionization mass spectrometry (TE-TIMS) methods were used to analyze individual zircon grains from samples PK-05-1081, PK-05-1050 and PK-06-1250.

#### **4.2.1 Sample processing and mineral separation**

Samples are crushed and specific mineral phases separated using conventional methods as follows. Samples are passed through a jaw crusher and pulverized with a disc mill. After crushing and milling, samples are passed over the Wilfley table and sieved to 70 mesh. Bromoform heavy liquid, initial Frantz magnetic, methylene iodide heavy liquid, and final Frantz magnetic mineral separations are performed to isolate distinct mineral fractions. Individual grains are hand-picked under a microscope, mounted, and filed down for cross-sectional viewing if warranted. For ID-TIMS methods, a selection of zircons are air abraded to remove zoned rims (after Krogh, 1982), re-examined under the microscope, and certain grains are selected for U-Pb analysis. Mineral dissolution and U-Pb isolation follow the procedure outlined by Krogh (1973) after which they are mounted together on rhenium filaments and placed into the mass spectrometer for analysis. Rather than air abrasion, the TE-TIMS method pre-heats individual zircon grains to evaporate and eliminate the effects of Pb loss in altered zones. Zircons are mounted in a silica glass and analyzed on the mass spectrometer following the procedure outlined by Davis (2008).

### **4.3 Sample Descriptions and U-Pb Results**

#### **4.3.1 Sample PK-05-1081: Bernic Lake Formation dacite (UTM 328559 5589623)**

Sample PK-05-1081 was collected from a sequence of massive to fragmental quartz- and feldspar-phyric dacite that occurs approximately 1 km north of Bernic Lake. This unit is part of the tholeiitic calc-alkaline volcanic pile that comprises the Bernic Lake Formation. The results will give an absolute age of volcanism, which can then be

compared with similar data collected from other volcanic sequences in the belt (e.g. Peterson Creek Formation), and allow for further refinement of the current stratigraphy.

The sample yielded an abundant zircon population of stubby, euhedral crystals, with sector zonation from clear to brownish hues and no evidence of cores (Figure 17). Zircons have uranium concentrations of ~200 ppm and Th/U values between 0.5 and 0.6. Three uncracked zircons were abraded and selected for analysis. Results of the analyses are shown in Table 1 and Figure 17-19. The analyses produced 3 near concordant data with average  $Pb^{207}/Pb^{206}$  ages of  $2724.6 \pm 1.1$  Ma (Figure 18). As no evidence of inheritance was noted in the sample, this age is interpreted as the age of volcanism of the dacite. TE-TIMS analyses on two zircon grains yielded average ages of  $2724.9 \pm 0.4$  Ma and  $2724.6 \pm 0.6$  Ma and are consistent with the interpretation of the ID-TIMS data (Figure 19).

#### **4.3.2 Sample PK-06-1250: Birse Lake granodiorite (UTM 327146 5587712)**

The sample is taken from the northern margin of the main body of the Birse Lake granodiorite on the south-central shore of Bernic Lake. The sample is a massive, homogeneous, medium- to coarse-grained quartz- and feldspar-phyric granodiorite that is intruded into the south panel MORB-type basalt. It differs slightly from other felsic intrusive rocks in the belt in that it contains a locally well-developed east-trending protomylonitic fabric that is consistent with the primary schistosity ( $S_2$ ) observed in volcanic rocks. Occasionally, thin zones of more intense deformation occur, and it is thus interpreted as being emplaced pre- to syn-tectonically. The sample was collected to constrain absolute age of “early” magmatism in the Bird River greenstone belt, the

Table 1. ID-TIMS data from sample PK-05-1081.

PK-05-1081 Bernic Lake Fm.  
dacite

No.	Fraction	Wt. (mg)	U (ppm)	Th/ U	Pb <sub>co</sub> <sub>m</sub> (pg)	<sup>207</sup> Pb/ <sup>204</sup> P <sub>b</sub> measure <sub>d</sub>	<sup>206</sup> Pb/ <sup>238</sup> U Age (Ma)	2σ	<sup>207</sup> Pb/ <sup>235</sup> U Age (Ma)	2σ	<sup>207</sup> Pb/ <sup>206</sup> P <sub>b</sub> Age (Ma)	2σ	Dis c (%)	ρ Conc.
dwd5091	1 Ab zr, eq, br	0.00	406	0.55	1.6	3635	2723.8	5.4	2727.8	2.6	2730.8	1.5	0.3	0.9475
dwd5092	1 Ab zr, eq, br	0.00	414	0.58	0.7	2236	2705.0	5.5	2720.1	2.6	2731.4	1.8	1.2	0.9148
dwd5093	1 Ab zr, eq, br	0.00	533	0.51	0.4	661	2725.6	6.4	2728.9	3.1	2731.4	2.1	0.3	0.9197

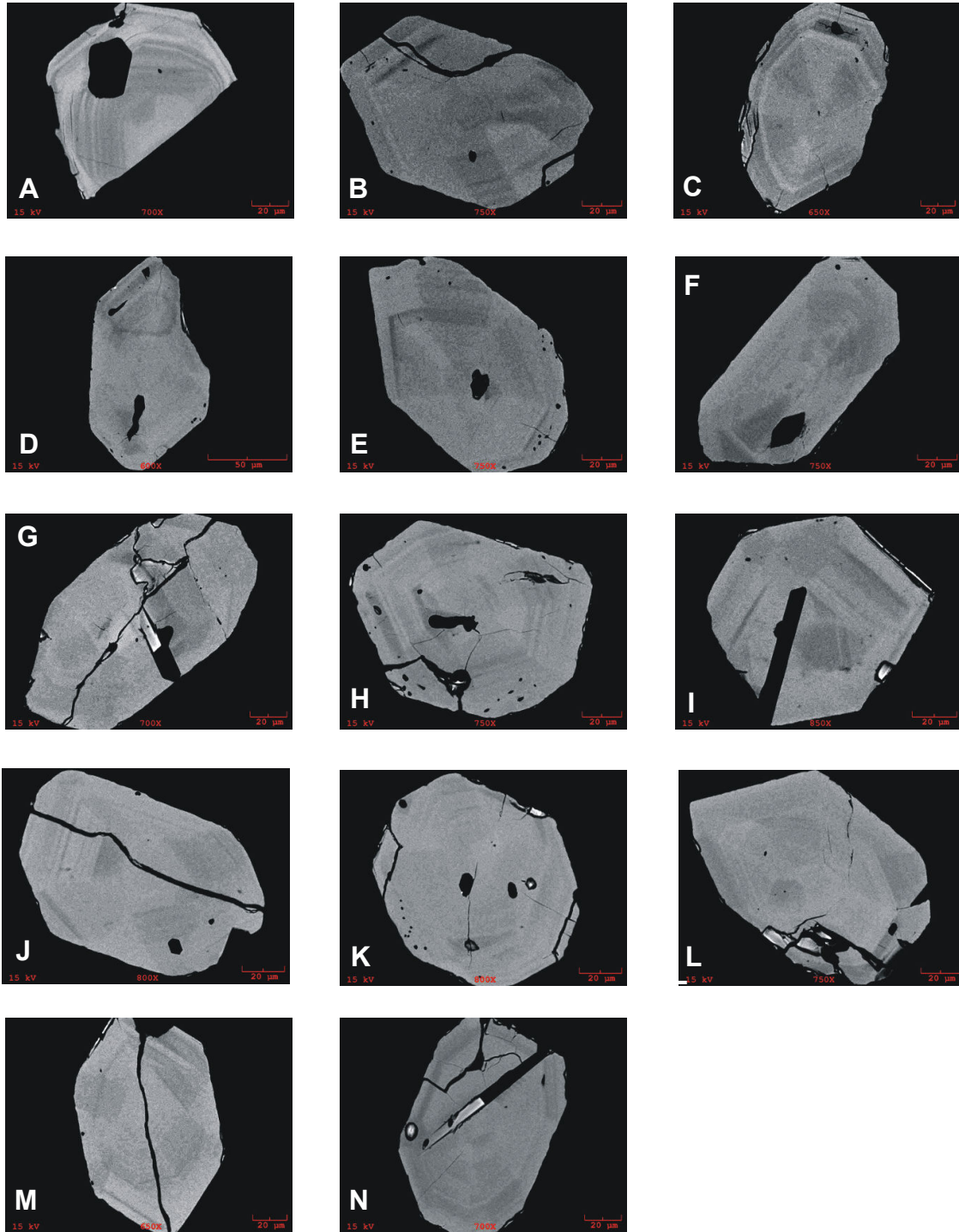


**Figure 17.** Electron microprobe BSE images of zircons collected from sample PK-05-1081.

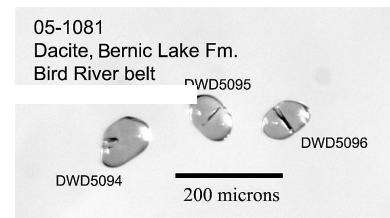
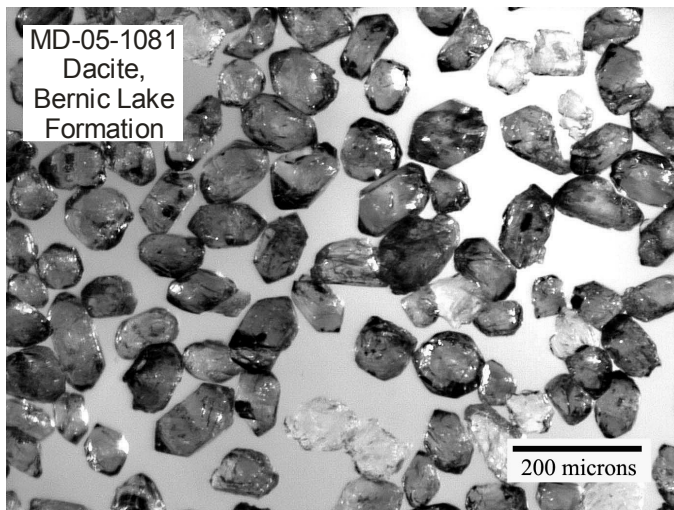
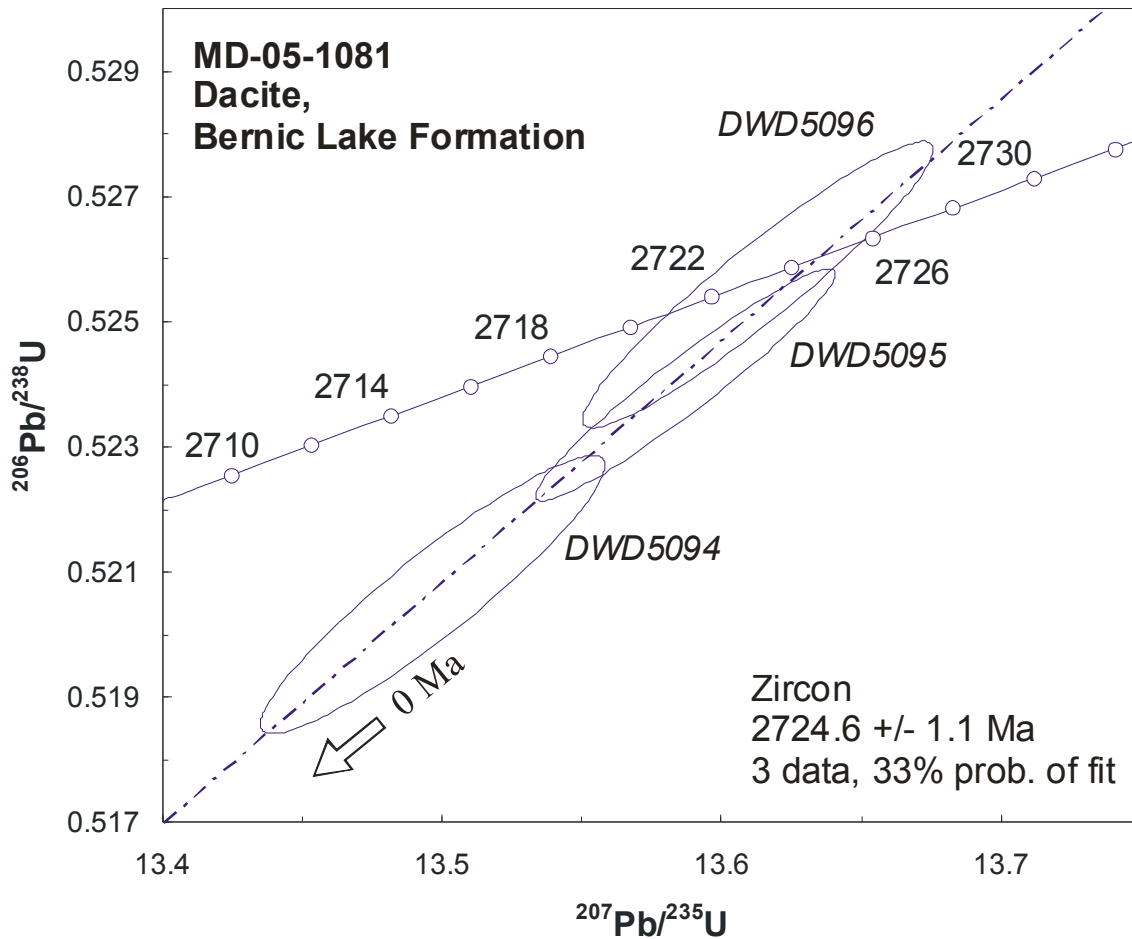


**Figure 18.** Concordia diagram showing ID-TIMS data from zircon collected from sample PK-05-1081. Lower images show zircon population after mineral separation (left) and the 3 air abraded zircon grains that were hand picked for analysis (right).

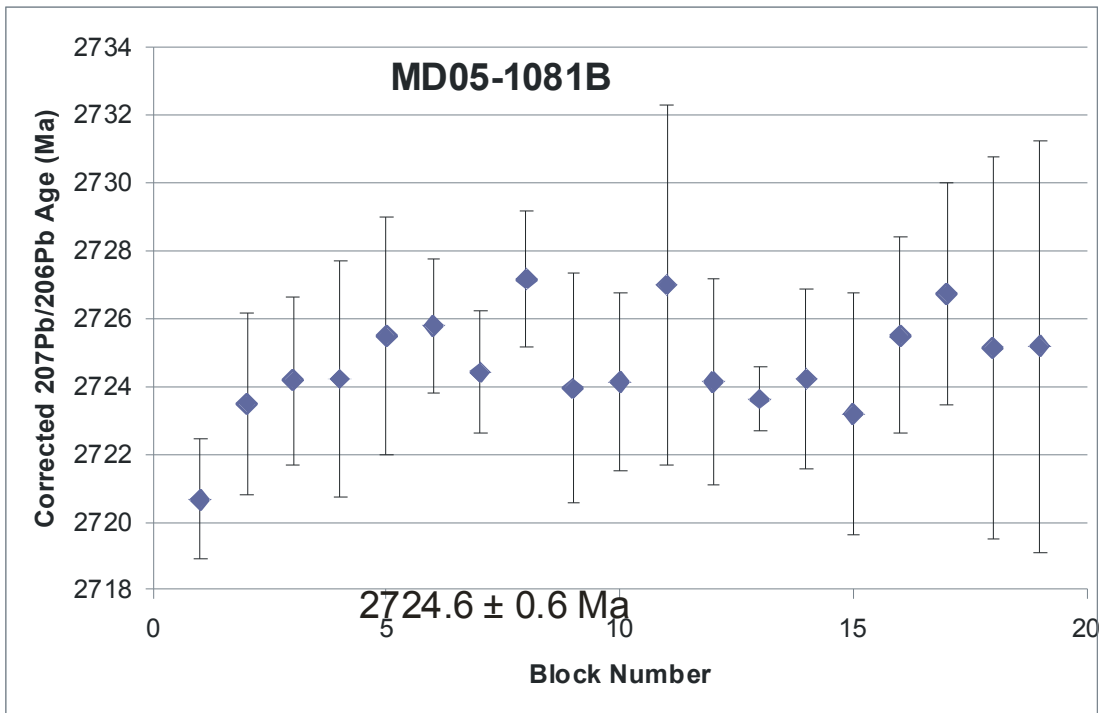
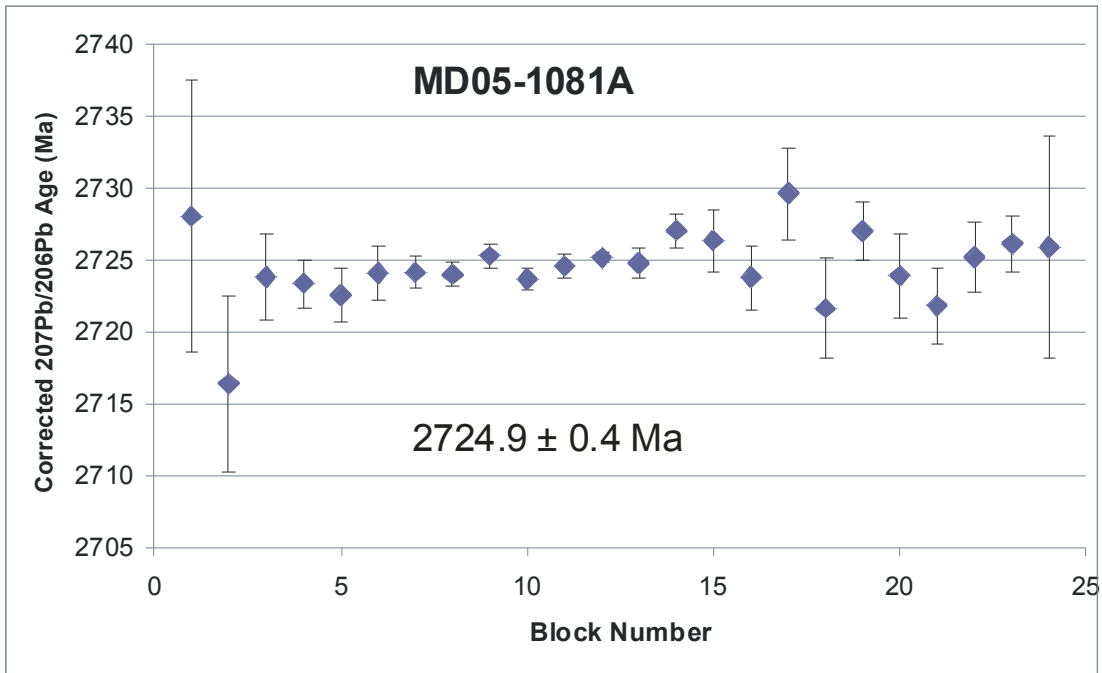


**Figure 19.**  $^{207}\text{Pb}/^{206}\text{Pb}$  age data from TE-TIMS analyses on zircon from sample PK-05-1081.

minimum age of the south panel MORB-type basalt, and the maximum age of D<sub>2</sub> deformation.

The sample yielded an abundant population of euhedral to subhedral zircons with equant to prismatic habits, a slight brownish colour, and occasional fluid inclusions. Internal normal zoning, uranium concentrations between 100 and 200 ppm, and Th/U ratios of approximately 0.5, are suggestive of a magmatic origin for the zircons. Four zircons from the sample were abraded and selected for analysis. Results of the analyses are shown in Table 2 and Figures 20 and 21. The analyses produced two overlapping data points (grains dwd5209 and dwd5212) that are within error of Concordia with Pb<sup>207</sup>/Pb<sup>206</sup> ages of  $2722.8 \pm 1.7$  Ma and  $2722.5 \pm 1.5$  Ma (Figure 20). The remaining two grains show slight discordance, however both are within error of the aforementioned overlapping concordant data. One grain (dwd1211) lies below Concordia (5.8% discordancy, Pb<sup>207</sup>/Pb<sup>206</sup> age  $2723.7 \pm 1.4$  Ma) and one grain (dwd1210) lies above (-0.3% discordancy, Pb<sup>207</sup>/Pb<sup>206</sup> age  $2723.8 \pm 1.4$  Ma). A regression line through all 4 data yields an upper intercept of  $2723.2 \pm 0.7$  Ma, interpreted to be the age of crystallization of the Birse Lake granodiorite. Two TE-TIMS analyses were conducted on zircon collected from the sample (Figure 21). One analysis yielded a stable age plateau with an average age of  $2723.0 \pm 0.2$  Ma. The second analysis showed a consistent increase in age throughout with an average age of  $2722.5 \pm 0.4$  Ma. The last 5 data, however, fit within error yielding an average age of  $2722.8 \pm 0.3$  Ma. These data are consistent with and support the interpretation from the ID-TIMS data.

Table 2. ID-TIMS data from sample PK-06-1251

PK-06-1250 Birse Lake pluton  
(granodiorite)

No.	Fraction	Wt. (mg)	U (ppm)	Th/ U	Pb <sub>co</sub> <sup>m</sup> (pg)	<sup>207</sup> Pb/ <sup>204</sup> Pb measure d	<sup>206</sup> Pb/ <sup>238</sup> U Age (Ma)	2σ	<sup>207</sup> Pb/ <sup>235</sup> U Age (Ma)	2σ	<sup>207</sup> Pb/ <sup>206</sup> Pb Age (Ma)	2σ	Disc c (%)	ρ Conc.
dwd520		0.00												0.9281
9	1 Ab zr, brn prism	2	181.3	0.49	0.4	6541	2718.2	5.4	2720.8	2.5	2722.8	1.7	0.2	8
dwd521		0.00												0.9552
0	1 Ab zr, brn, eq, a few incl	2	122.5	0.55	0.5	4226	2711.5	5.5	2718.6	2.6	2723.8	1.4	0.5	7
dwd521		0.00												0.9322
1	1 Ab zr, brn, eq, a few incl	2	108.5	0.53	0.5	3268	2722.4	4.4	2723.1	2.2	2723.7	1.4	0.1	4
dwd521		0.00												0.9557
2	1 Ab zr, brn, eq, a few incl	2	144.6	0.56	0.2	8475	2729.3	4.9	2725.4	2.4	2722.5	1.3	-0.3	5

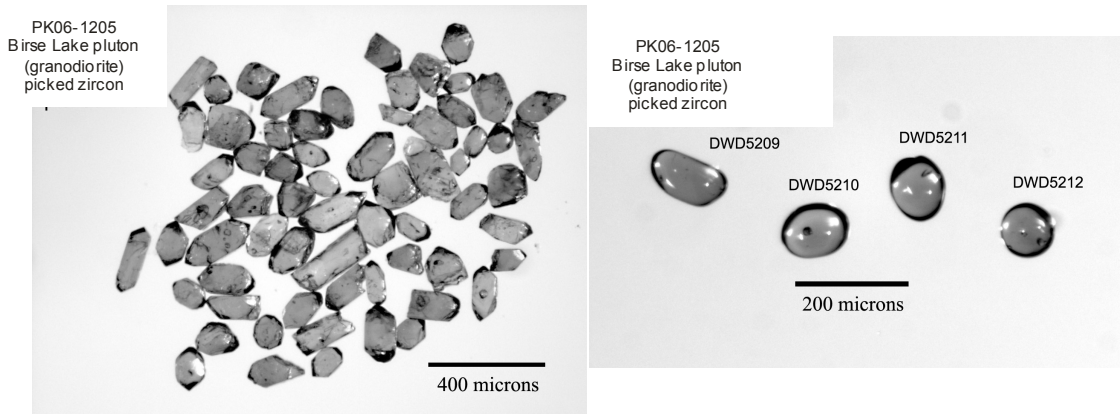
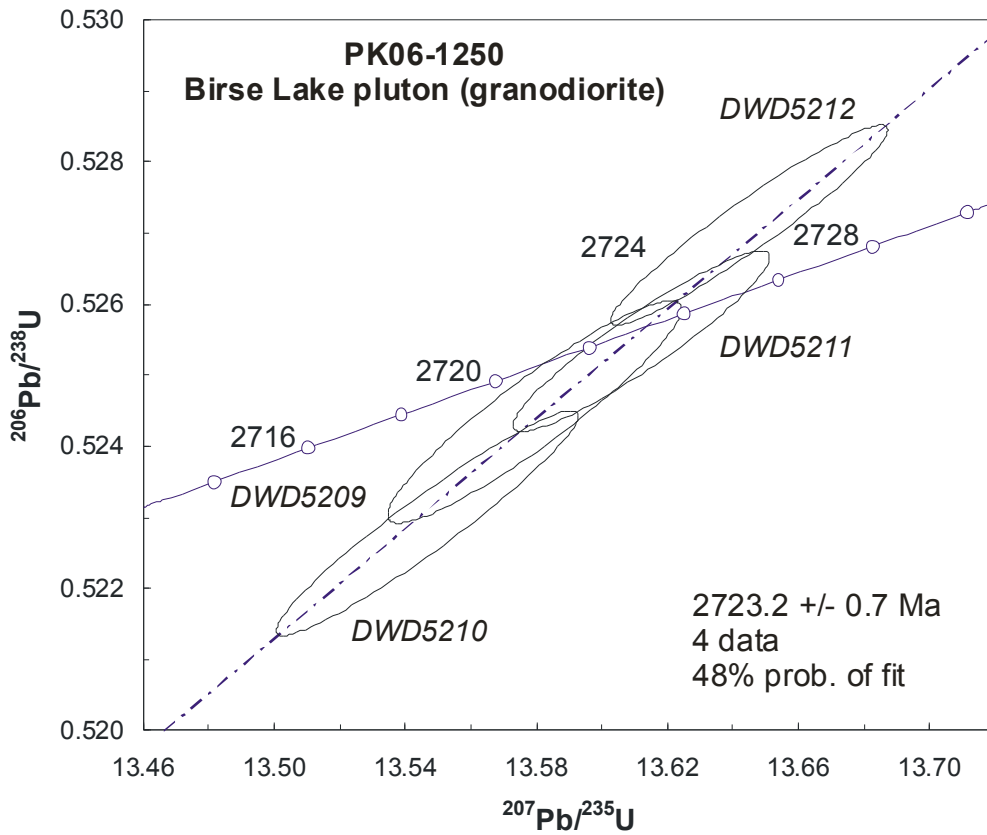


**Figure 20.** Concordia diagram showing ID-TIMS data from zircon collected from sample PK-06-1250. Lower images show picked zircon population after mineral separation (left) and the 4 air abraded zircon grains that were hand picked for analysis (right).

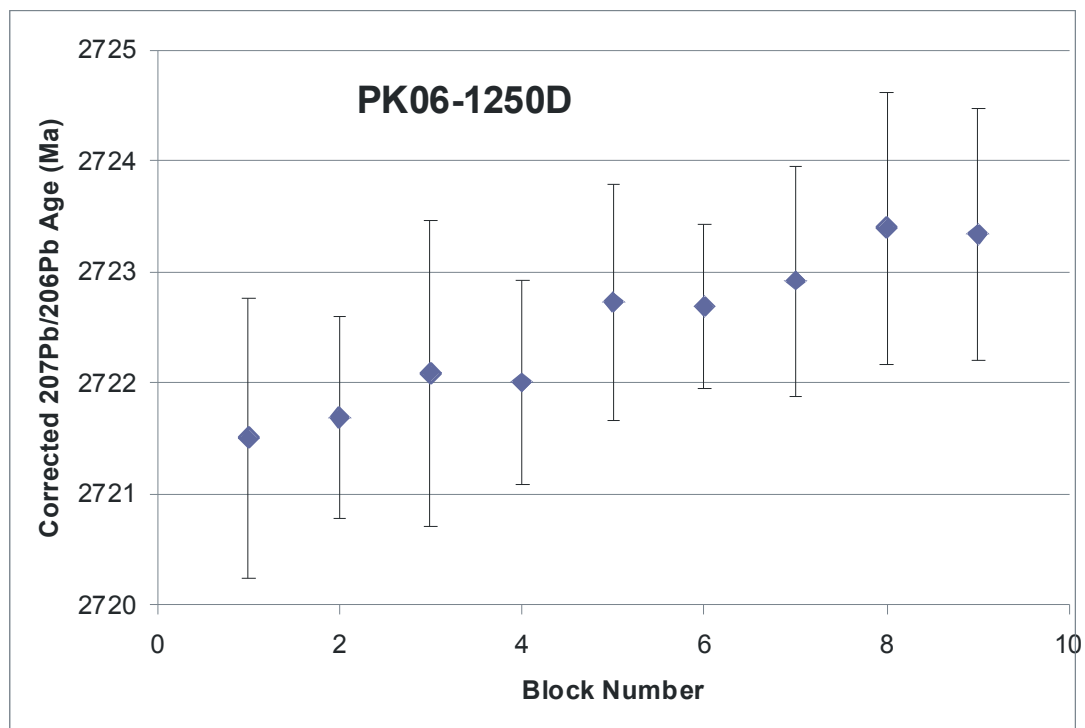
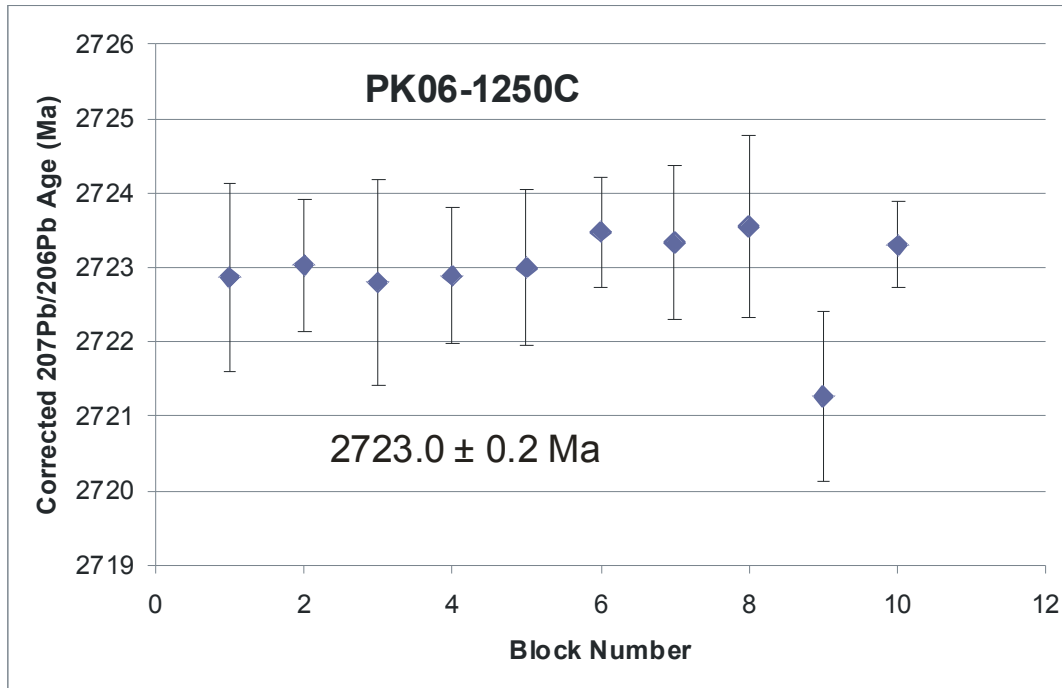


**Figure 21.**  $^{207}\text{Pb}/^{206}\text{Pb}$  age data (corrected) from TE-TIMS analyses on zircon from sample PK-06-1250.

### 4.3.3 Sample PK-06-1197: Tanco gabbro (UTM 325002 5589349)

This sample of the Tanco gabbro was collected on the northwest shore of Bernic Lake. It is part of a series of outcrops that show the variable nature of the mafic intrusive rocks that host the Tanco pegmatite. At this location, a segregation of pegmatitic gabbro with plagioclase and hornblende crystals up to 3 cm occurs. Exposed contacts are diffuse and gradational into a coarse- to medium-grained gabbro with equigranular to subophitic textures. This sample will offer a maximum age for the Tanco pegmatite if data from collected pegmatites (samples PK-05-1050 and PK-06-1250) prove to be poor. Furthermore, the genetic relationship between mafic volcanic rocks of the Bernic Lake Formation and the Tanco gabbro will be determined (i.e. syn- versus post-volcanic intrusion).

The sample yielded small, stubby to equant, clear to pale brown zircons and zircon fragments with rare inclusions and variably cracked and altered rims. As with samples PK-05-1081 and PK-06-1251, the characteristics of the zircons (uranium concentrations between 150 and 350 ppm, Th/U ratios between 0.45 and 0.54) are indicative of a magmatic source. Three zircons (dwd5241, dwd5242, dwd5243) from the sample were abraded and selected for analysis. Results of the analyses are shown in Table 3 and Figure 22. The analyses of the zircons produced three overlapping data that are concordant to slightly discordant (0.2-0.3% discordancy) with consistent  $Pb^{207}/Pb^{206}$  ages (Figure 22). A regression line through the 3 analyses has an upper intercept of  $2723.1 \pm 0.8$  Ma. Given the nature of the zircon grains analyzed and the precision of the data, this age is interpreted to represent the age of crystallization of the Tanco gabbro.

Table 3. ID-TIMS data from sample PK-06-1197.

PK-06-1197 Tanco gabbro														
No.	Fraction	Wt. (mg)	U (ppm)	Th/U	Pb <sub>co</sub> <sup>m</sup> (pg)	<sup>207</sup> Pb/ <sup>204</sup> Pb <sub>b</sub> measure <sup>d</sup>	<sup>206</sup> Pb/ <sup>238</sup> U Age (Ma)	2σ	<sup>207</sup> Pb/ <sup>235</sup> U Age (Ma)	2σ	<sup>207</sup> Pb/ <sup>206</sup> Pb <sub>b</sub> Age (Ma)	2σ	Disc (%)	P Conc.
dwd524		0.00												0.9555
1	1 Ab zr frag, eq, brn/cir, incl	6	158.4	0.54	2.6	11747	2716.6	5.2	2720.3	2.6	2723.1	1.4	0.3	8
dwd524		0.00												0.9600
2	1 Ab rnd zr, eq, cir	4	339.2	0.47	1.7	24331	2717.5	5.5	2720.8	2.6	2723.3	1.3	0.3	7
dwd524		0.00												0.9548
3	1 Ab rnd zr, stubby, brn, crk	5	268.1	0.45	1.3	32353	2718.5	5.1	2720.9	2.5	2722.7	1.3	0.2	4

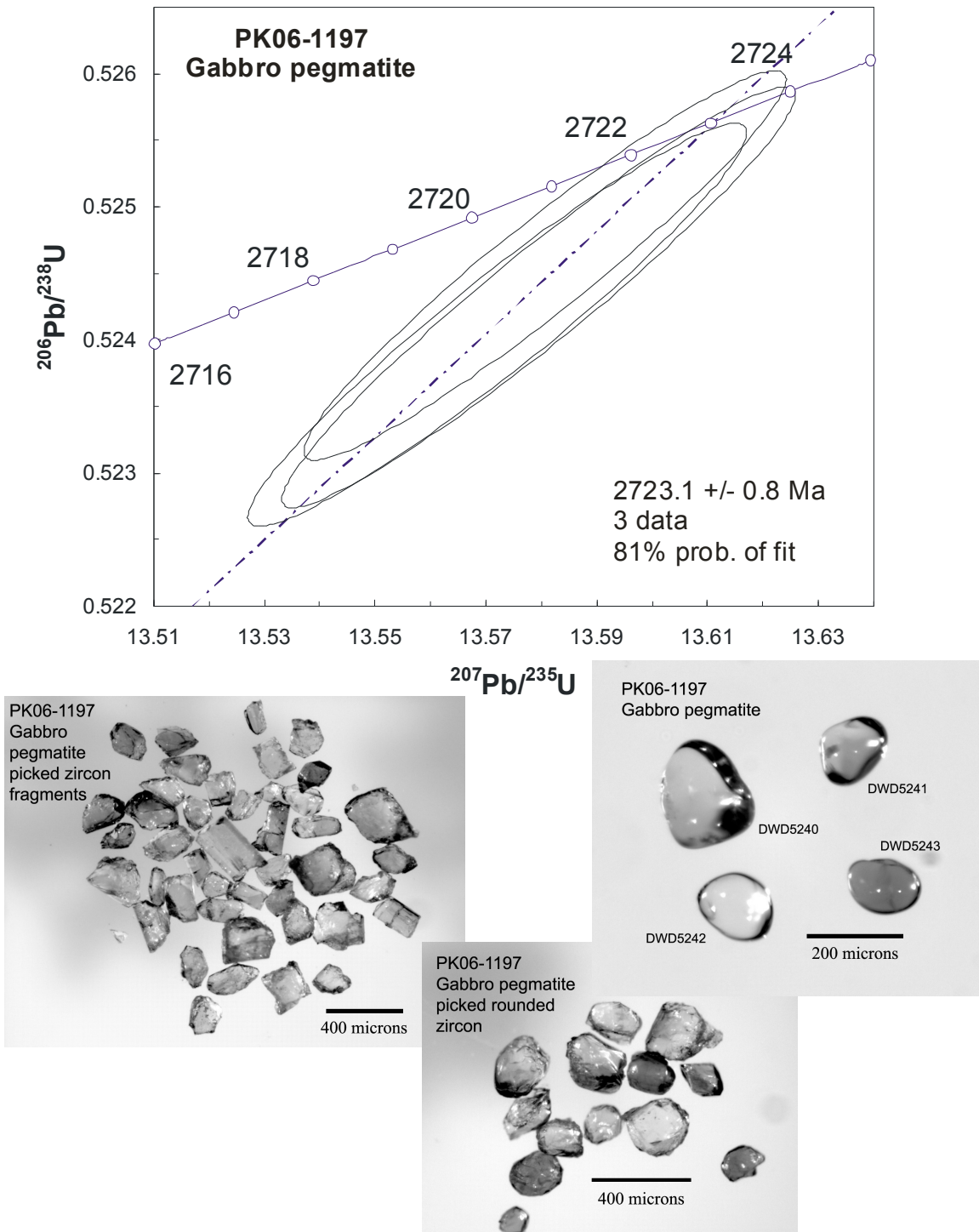


**Figure 22.** Concordia diagram showing ID-TIMS data from zircon collected from sample PK-06-1197. Lower images show picked zircon fragments (left), picked rounded zircon (lower middle) and the 4 air abraded zircon grains that were hand picked for analysis (right).

#### **4.3.4 Sample PK-05-1050: Oompa Loompa pegmatite (330443 5588432)**

Pegmatite (Oompa Loompa) sample was collected approximately 500 meters east of Bernic Lake where the majority of the Bernic Lake pegmatite group occurs. It is emplaced within, and crosscuts the tectonic fabric of the North Bernic Lake Shear Zone (Figure 16). The pegmatite shows features consistent with passive crystallization such as euhedral feldspar intergrowths oriented perpendicular to the pegmatite contacts, however, it is deformed and displays folding and incipient boudinage that interpreted to record increments of  $G_3$  strain. This pegmatite is thus interpreted to have been emplaced during the late stages of  $G_3$  deformation. The pegmatite displays a crude zoning, and the sample was collected from the central zone where quartz is more abundant. This sample, in conjunction with a pre-existing age of the Tanco pegmatite (Baadsgaard and Cerny, 1993) will help to determine the age relationship between fracture-hosted and shear-hosted pegmatites around the Tanco mine site and will also place constraints on the age of  $G_3$  deformation.

The zircon population consists of stubby, subhedral to euhedral grains with rounded edges and corners. The average size of zircon grains is approximately 200  $\mu\text{m}$  in width, with aspect ratios ranging between 1.5 and 2. All zircons collected and analyzed from the sample show very low Th/U values, which is a feature typical of pegmatite zircon. Figure 23 shows photomicrographs and backscattered electron images of mounted grains. Two grains display normal zoning throughout, however, a thin discontinuous rim of high U zircon (bright colour) is present. Irregular zone boundaries observed in one grain are indicative of recrystallization. Dark patches around the rims of all grains reflect areas of secondary alteration.

PK05-1050  
Granitoid pegmatite,  
shear-zone hosted  
zircon

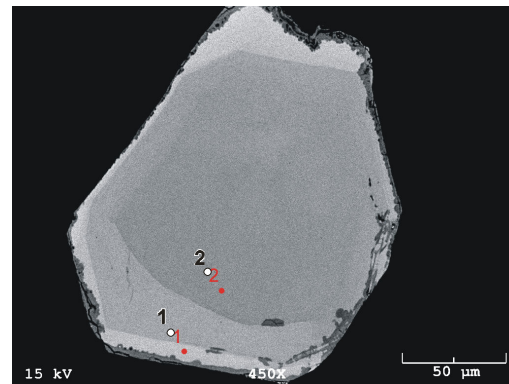
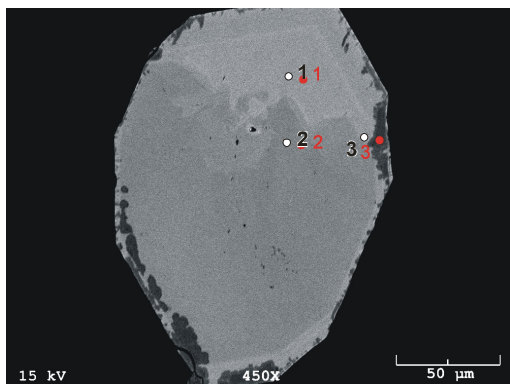
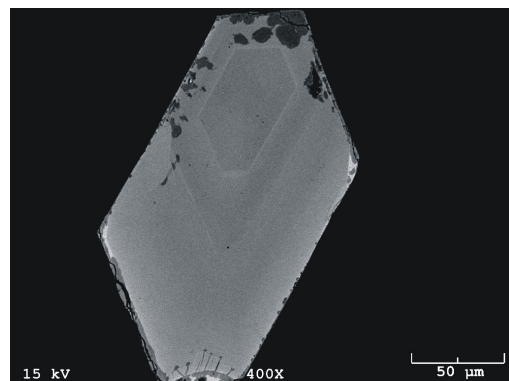
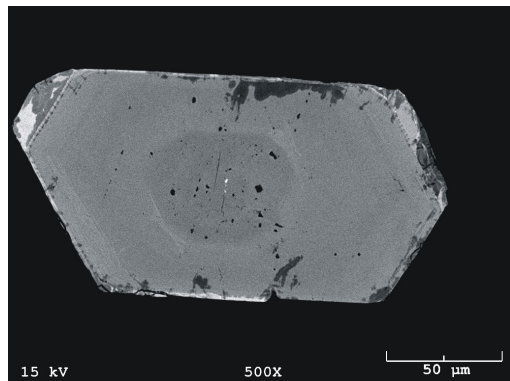
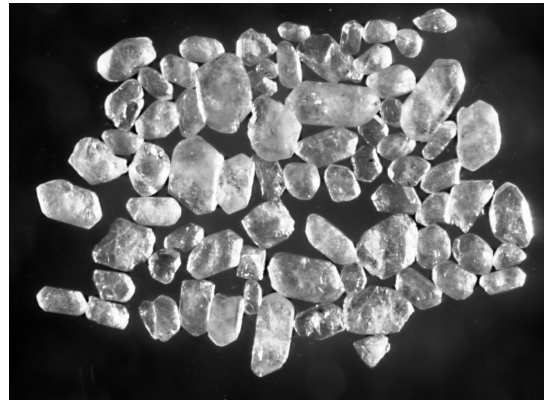
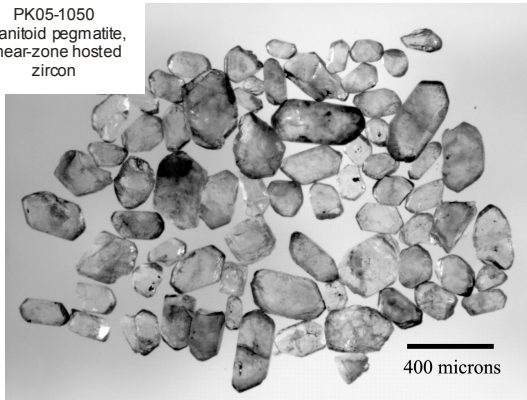


**Figure 23.** Photomicrographs (upper two) and electron microprobe BSE images (lower four) showing zircon collected from sample PK-05-1050.

Three zircon grains (A, B, C) were selected from the sample for analysis by TE-TIMS. Data and results from the analyses are listed in Figure 24. Grain A did not emit very well, and shows a consistent increase in age with increasing intensity. Furthermore, an increase in common Pb is also observed at higher intensities, suggesting that thermal pre-treatment did not remove all the Pb from the altered zones prior to analysis. The most precise datum from grain A yielded an age of  $2651.4 \pm 1.0$  Ma. Grain B emitted well and gives a consistent age of  $2650.7 \pm 0.2$  Ma. Grain C also emitted well, however, a variance of ages were recorded from the data. Ages start at  $2651.8 \pm 2.9$  Ma at lower intensities, increase with increasing intensity to a peak of  $2657.8 \pm 1.2$  Ma, and then decrease with increasing intensity to  $2643.5 \pm 2.0$  Ma. Emission at higher intensities was too low to measure precisely. The grain had negligible amounts of common Pb, which suggests that the younger ages do not result from alteration. The caveat of this is that the possibility exists of multiple phases of zircon growth in the sample. If this were the case, however, the youngest ages should have been recorded towards the beginning of the analysis at lower intensities, as the younger phase should have overgrown the older phase.

In addition to zircon, the sample also yielded an abundant fraction of columbite crystals, selected for analysis by ID-TIMS. The majority of tantalite grains were somewhat altered, but nonetheless gave highly radiogenic data (Table 4). Of the three grains analyzed, one grain was leached in a weak solution of HF, and produced a concordant age of  $2647 \pm 1.0$  Ma (Figure 25). The two grains not leached in HF had varying amounts of discordance.

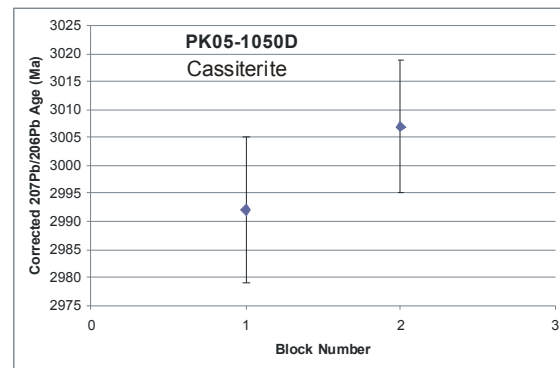
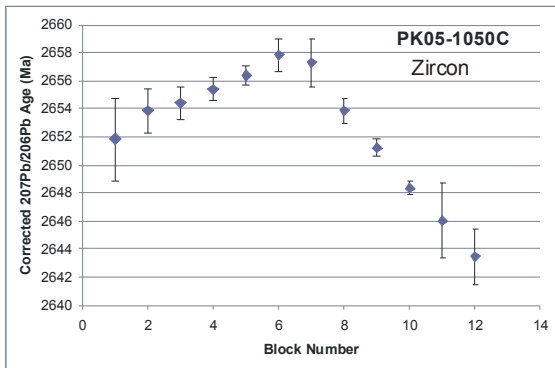
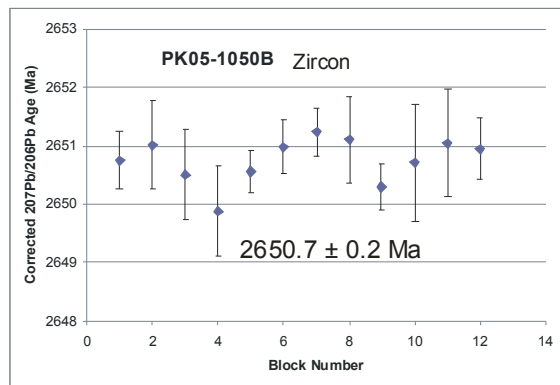
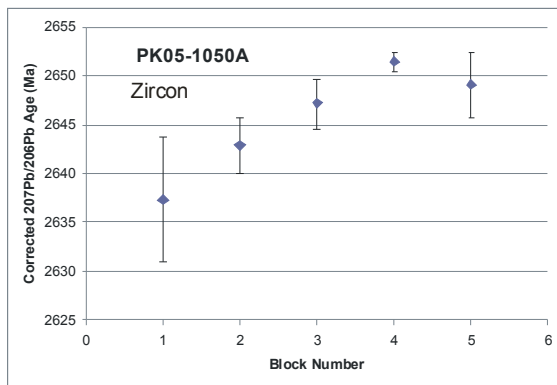
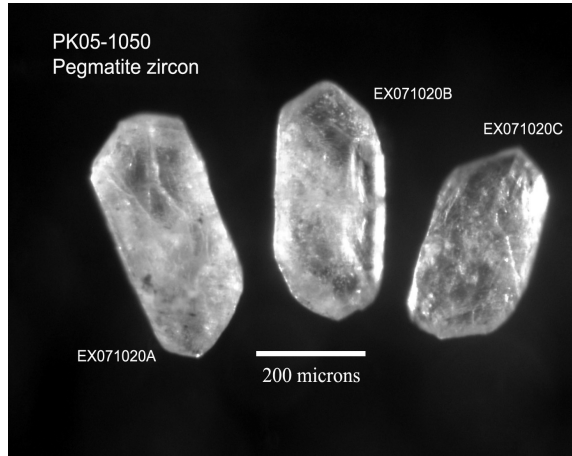


**Figure 24.**  $^{207}\text{Pb}/^{206}\text{Pb}$  age data (corrected) from TE-TIMS analyses on zircon and cassiterite (lower right) from sample PK-05-1050.

Table 4. ID-TIMS data from sample PK-05-1050.

PK-05-1050 Shear-hosted pegmatite														
No.	Fraction	Wt. (mg)	U (ppm)	Th/ U	Pb <sub>co</sub> <sub>m</sub> (pg)	<sup>207</sup> Pb/ <sup>204</sup> P b measure d	<sup>206</sup> Pb/ <sup>238</sup> U Age (Ma)	2σ	<sup>207</sup> Pb/ <sup>235</sup> U Age (Ma)	2σ	<sup>207</sup> Pb/ <sup>206</sup> P b Age (Ma)	2σ	Dis c (%)	ρ Conc.
dwd5274	1 flat xstal, clbt	36	619	0.01	11.4	9469	2554.3	6.8	2601.3	3.3	2638.2	1.3	3.8	4
dwd5275	1 flat xstal, clbt	24	1095	0.01	24.9	5160	2581.9	4.7	2645.3	2.8	2647.4	1.4	3.1	3
dwd5286	1 frag clbt, leached	15	79	0.01	2.9	2243	2642.7	5.9	2619.8	2.4	2649.2	1.6	0.2	0

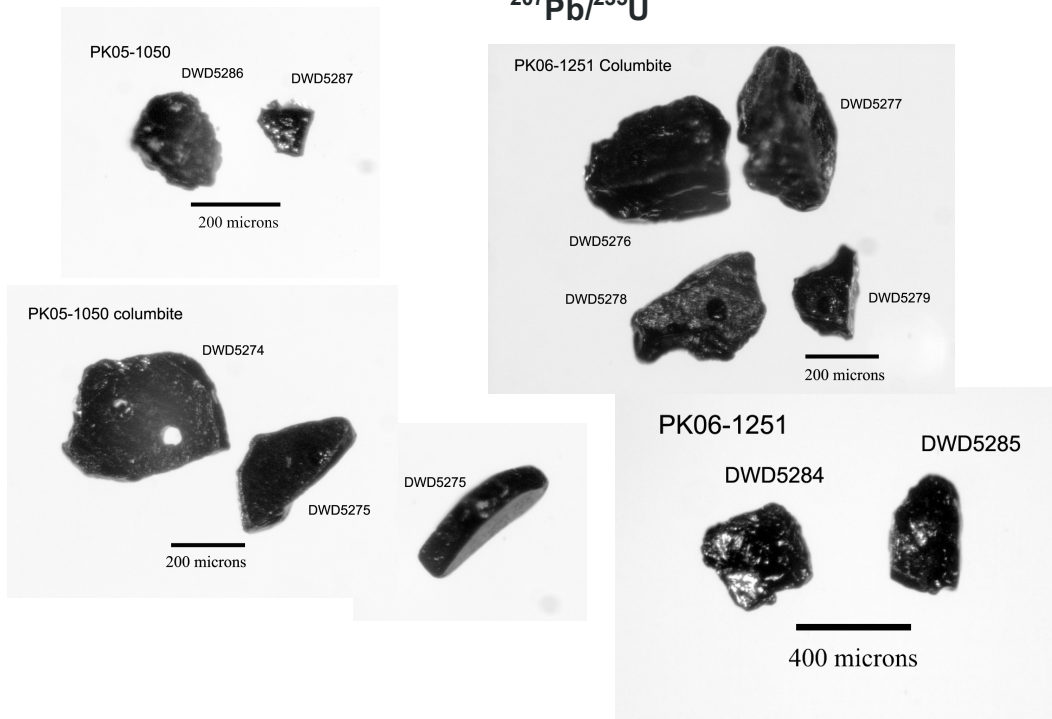
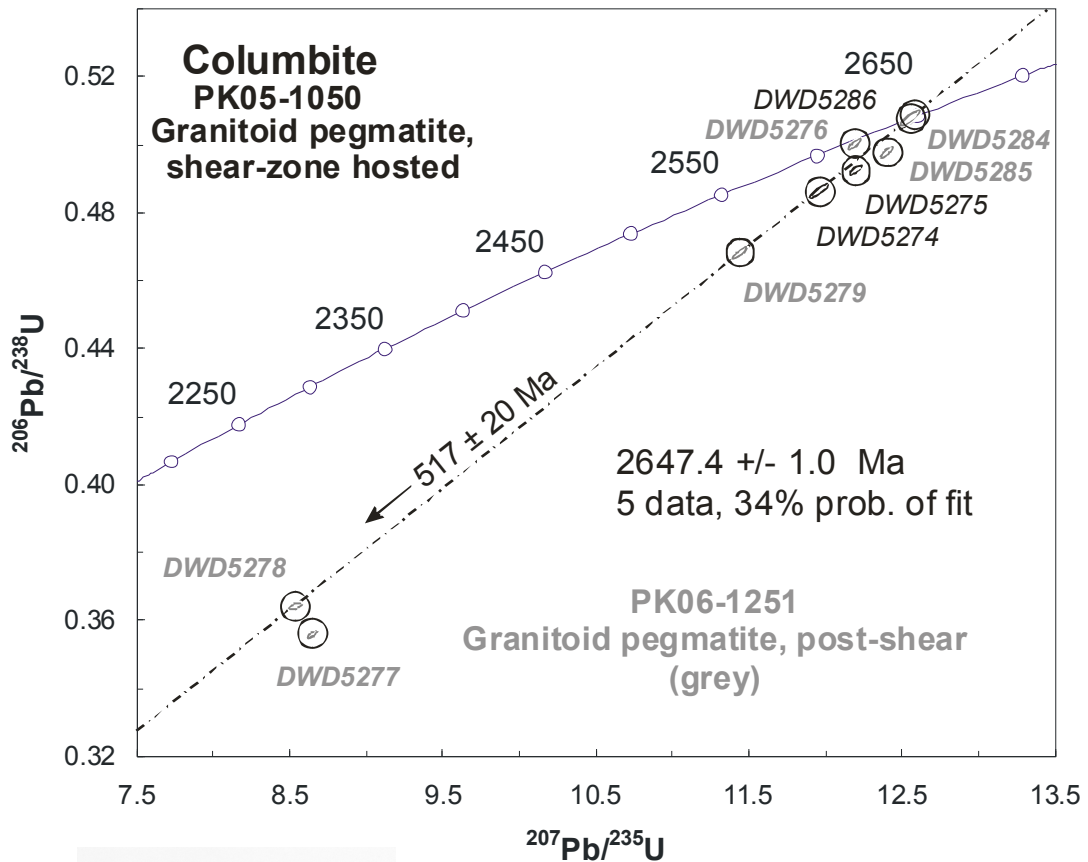


**Figure 25.** Concordia diagram showing ID-TIMS data from columbite collected from sample PK-05-1050 and PK-06-1251. Lower images show picked columbite fragments from each sample.

#### **4.3.5 Sample PK-06-1251: Fracture-hosted pegmatite (UTM 325807 5590495)**

This sample was collected from an outcrop approximately 1 km northwest of the Tanco mine along a road that leads around an old tailings pile. The pegmatite occurs as a narrow dike (approximately 1 meter wide) oriented 290°/28°. It is intruded into strongly recrystallized mafic rocks that occur immediately north of the contact between the Tanco gabbro and basalt of the Bernic Lake Formation. Pegmatite contacts are straight, very sharp, and crosscut the schistosity ( $S_2$ : 127°/86°). The pegmatite is similar in appearance and mineralogy to offshoots of the Tanco pegmatite “wall zone” that were observed underground. This sample, in conjunction with PK-05-1050 will determine the age relationship between fracture-hosted and shear-hosted pegmatites around the Tanco mine site and will also serve to reinforce the 2640 +/- 7 Ma age for the Tanco pegmatite (Baadsgaard and Cerny 1993).

The sample yielded no zircon, however abundant, variably altered, columbite was present. 6 tantalite grains, 2 of which were leached in weak HF, were selected for analysis by ID-TIMS. Results are shown in Table 5 and Figure 26. The 2 leached grains produced concordant data, however the ages were not consistent with one another (ca. 2647 Ma and 2623 Ma respectively). The 4 grains not leached in HF all show varying degrees of discordancy.

#### **4.4 Interpretation of U-Pb Geochronology Data**

Three of the samples collected (PK-05-1081, PK-06-1197, and PK-06-1250) returned data that are consistent with each other ( $2724.6 \pm 1.1$  Ma,  $2723.1 \pm 0.8$  Ma, and  $2723.2 \pm 0.7$  Ma respectively). The age of eruption of felsic volcanic rocks in the Bernic

Table 5. ID-TIMS data from sample PK-06-1251.

**PK-06-1251 Fracture-hosted  
pegmatite**

No.	Fraction	Wt. (mg)	U (ppm)	Th/ U	Pb <sub>co</sub> (pg)	<sup>207</sup> Pb/ <sup>204</sup> P b measure d	<sup>206</sup> Pb/ <sup>238</sup> U Age (Ma)	2σ	<sup>207</sup> Pb/ <sup>235</sup> U Age (Ma)	2σ	<sup>207</sup> Pb/ <sup>206</sup> P b Age (Ma)	2σ	Dis c (%)	ρ Conc.
dwd527														0.9528
6	1 frag clbt	148	59	0.00	8.3	5335	2614.6	5.3	2619.4	2.6	2623.1	1.4	0.4	9
dwd527														0.8630
7	1 frag clbt	143	71	0.00	60.7	590	1963.1	3.5	2301.9	2.4	2618.0	2.2	28.9	1
dwd527														0.6274
8	1 frag clbt	51	138	0.01	114.9	246	2002.4	3.5	2290.0	3.2	2557.6	4.6	25.9	4
dwd527														0.9270
9	1 frag clbt	11	155	0.00	9.0	898	2475.5	5.1	2559.9	2.6	2627.5	1.8	7.0	1
dwd528														0.9704
4	1 fresh frag clbt, leached	85	38	0.00	10.9	1527	2646.4	7.0	2646.5	3.3	2646.7	1.4	0.0	1
dwd528														0.9523
5	1 fresh frag clbt, leached	58	62	0.00	3.8	5156	2603.8	5.0	2634.8	2.5	2658.8	1.4	2.5	0

Lake Formation is constrained by sample PK-05-1081. The quartz- and feldspar-phyric dacite that was dated occurs in a conformable relationship with basaltic mafic volcanic rocks. The age data  $2724.6 \pm 1.1$  Ma can therefore be used as a representation of the age of volcanism of the entire formation. Samples PK-06-1197 and PK-06-1250, from the Tanco gabbro and Birse Lake granodiorite, indicate that these rocks are likely parts of the subvolcanic system of the Bernic Lake Formation, with the Birse Lake granodiorite feeding the felsic to intermediate volcanics and the Tanco gabbro feeding the mafic volcanics. Field observations are consistent with this data, in that a series of quartz-and feldspar-phyric dykes can be traced northward from the main body of the Birse Lake granodiorite in the map area, and irregular fingers of the Tanco gabbro extend eastward into the mafic volcanic pile.

Leached columbite from pegmatite samples PK-05-1050 and PK-06-1251 produced 2 overlapping data (one from each sample) at ca. 2647 Ma. A regression line derived from these data and selected un-leached, discordant columbite from both samples has an upper intercept consistent with this at  $2647.4 \pm 1.0$  Ma. A third leached columbite from the latter sample yielded an ambiguous concordant age of 2623 Ma. The best data from TE-TIMS analyses of zircon from sample PK-05-1050 yielded a slightly older age ( $2650.7 \pm 0.2$  Ma) than that recorded from columbite grains. The range in ages across the 3 TE-TIMS analyses ( $2651.4 \pm 1.0$  Ma,  $2651.8 \pm 2.9$  Ma,  $2643.5 \pm 2.0$  Ma), however, suggests that there may be multiple phases of zircon growth.

Given the available data, the age of crystallization of the pegmatites sampled is interpreted to be  $2647.4 \pm 1.0$  Ma on the basis of the tantalite regression data. The deformation of sample PK-05-1050 observed in outcrop, as well as the spatial association

of the Bernic Lake pegmatite group as a whole to the NBLSZ suggests that it acted as a pathway for pegmatitic melt to ascend from depth. If deformation along the NBLSZ was sustained, then multiple pulses of pegmatitic fluid are likely to have exploited it throughout its history, yielding pegmatites with slight variations in crystallization age. It is possible, therefore, that the zircon grains in sample PK-05-1050 originated from an earlier pulse and became entrained in the sample as it passed through the NBLSZ prior to emplacement.

If the columbite regression is taken as the age of crystallization of pegmatite samples PK-05-1050 and PK-05-1251, it remains necessary to resolve the concordant tantalite date ca. 2623 Ma. Based on the fact that Ta-oxides in the Tanco pegmatite occur in association with both primary magmatic zones and secondary alteration zones, a study conducted by Van Lichtenvelde et al. (2007) was designed to investigate the relative influence of magmatic versus metasomatic tantalum mineralization in the Tanco pegmatite. The authors concluded that although primary magmatic processes were responsible for the majority of tantalum mineralization at Tanco, late fluids could have been in part responsible for secondary Ta-oxide crystallization (Von Lichtevelde et al., 2006). The columbite age 2623 Ma, therefore, may represent a phase of metasomatic mineralization that post-dates the emplacement and primary crystallization of the pegmatite.

## Chapter 5

### Emplacement model for the Bernic Lake pegmatite group

#### 5.1 Structural Associations of the Bernic Lake Pegmatite Group

Pegmatite groups (including the Bernic Lake pegmatite group) in the Bird River greenstone belt show strong spatial associations to large, belt-scale fault structures that often mark structural boundaries between adjacent tectonostratigraphic formations (Figure 26). The tectonic juxtaposition of lithologies across these structures corresponds to the major deformation event  $G_2$ . In the case of the Bernic Lake group, pegmatites are localized along an east-west trend in close proximity to the NBLSZ, which separates MORB-type basalt to the south from the Bernic Lake Formation to the north. In some instances (e.g. Oompa Loompa pegmatite), pegmatites occur within the NBLSZ. Although passive crystallization is apparent (sharp contacts with rims of tourmaline and intergrown blocky feldspar perpendicular to pegmatite margins), the Oompa Loompa pegmatite is folded and boudinaged in a manner consistent with  $G_2$  shearing. The Tanco pegmatite, however, shows only ambiguous evidence of early, ductile deformation in the form of upright folds in the aplitic albite zone. These folds are similar in style and orientation to meso-scale upright  $F_2$  folds observed in outcrop elsewhere in the Bernic Lake Formation, but cannot be conclusively linked to  $G_2$  deformation. The Tanco pegmatite is emplaced exclusively along a conjugate fracture set that occurs in the Tanco gabbro. The fracture set hosting Tanco however, is inconsistent with, and is overprinted by late fracture system(s) in the area. Kinematic analysis of the Tanco-hosting fracture set indicates that it was formed during NNW-SSE directed subhorizontal shortening with predominantly vertical extension. This orientation is in agreement with

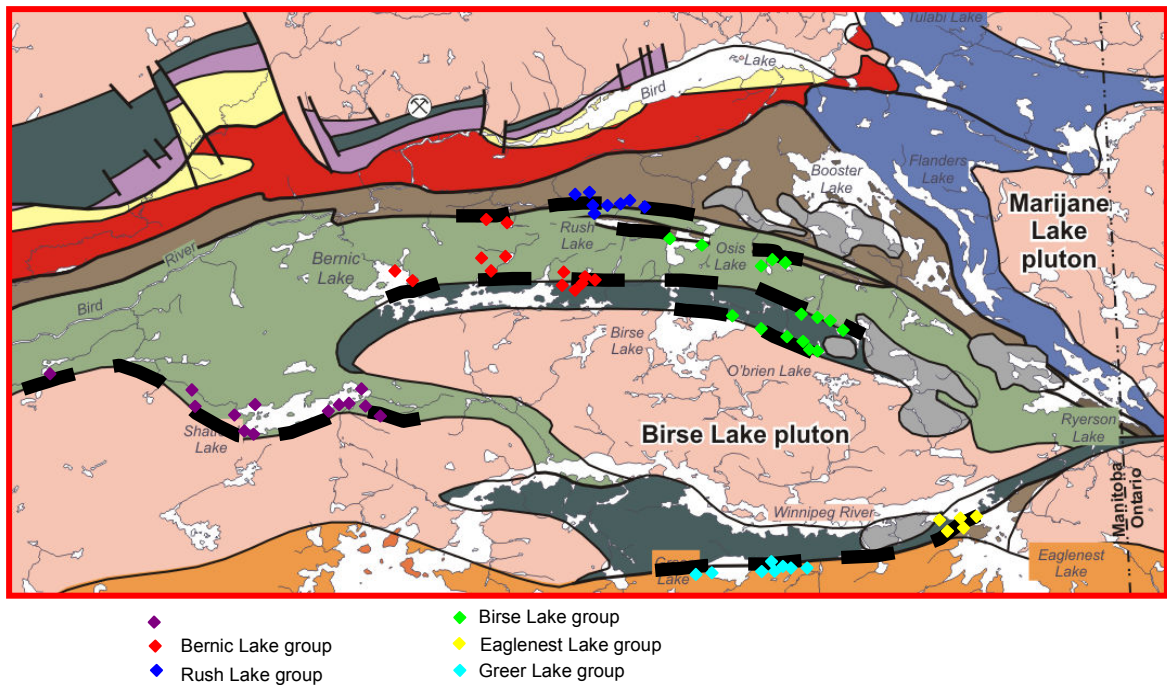


**Figure 26.** Simplified geological map of the Bird River greenstone belt showing the spatial association of 6 pegmatite groups (small diamonds) of the Winnipeg River pegmatite field to major, formation-bounding shear zones.

observations from  $G_3$  fabric elements which trend approximately  $070^\circ$ - $085^\circ$ , and the conjugate fractures are therefore interpreted as  $G_3$  structures. Furthermore, there is strong evidence (particularly east of Bernic Lake) that the NBLSZ was reactivated during  $G_3$  deformation. This being the case, and given the geochemical affiliations between the Tanco pegmatite and those occurring east of Bernic Lake, deformation observed in the Oompa Loompa pegmatite likely resulted in response to and records increments of  $G_3$  strain.

The majority of pegmatites (by number) in the Bernic Lake pegmatite group occur in the area east of Bernic Lake and are emplaced within, or within close proximity to, the NBLSZ. In certain exposures (e.g. the Oompa Loompa pegmatite) pegmatites display clear evidence of having undergone some degree of ductile deformation. They are folded and show correlative incipient boudinage. In other documented pegmatites in the area, these features are not manifest in surface exposures, however drill hole data has shown that they pinch and swell down dip (Lenton, 1979). The majority of pegmatites and pegmatitic granites in the belt are concentrated around large shear zones (Cerny et al. 1981), which suggests that these structures acted as pathways for granitic magma ascending from depth during  $G_3$  deformation. The large concentration of pegmatites along the NBLSZ east of Bernic Lake, rather than along its entire length, is likely due to the ESE orientation in this particular area (the NBLSZ trends E-W and ENE further to the west) where it is preferentially reactivated. Under the conditions of  $G_3$  deformation, the principal shortening axes are NNW-SSE and subhorizontal. In such a stress field, subvertical planes oriented ENE (such as the NBLSZ, western Bernic Lake) are nearly perpendicular to the shortening axes and would be subjected to compression with limited

simple shear components. Planes oriented oblique to the shortening axes (NBLSZ eastern Bernic Lake), have attitudes that favour reactivation by increasing the amount of simple shear on the plane. Increasing the obliquity of the plane with respect to the shortening axes (NBLSZ east of Bernic Lake) further increases the simple shear component and promotes a greater degree of reactivation. Pegmatites are located to the east of Bernic Lake where the orientation of the NBLSZ is at a higher angle to the inferred shortening axes and is more favourable for reactivation, thus allowing for the creation of more pathways through dilation and a greater volume of pegmatite intrusion. Furthermore, a right lateral warping in the NBLSZ in the area acts as a releasing bend, effectively increasing the dilational space available during deformation, creating domains of low pressure, and allowing for hydraulic pumping of pegmatitic melt into the created voids.

## **5.2 Temporal Associations of the Bernic Lake Pegmatite Group**

According to mapping by Duguet et al. (2005, 2006), pulses of granitic and pegmatitic magmatism throughout the belt are coeval with  $G_3$  deformation. In the northeastern corner of the belt, this is most evident by the emplacement of the Marijane granite in the nose of a large  $F_3$  fold structure (Duguet, 2005). The Marijane granite has been dated (U-Pb analysis on monazite) and yielded an age of  $2645.6 \pm 1.3$  Ma, which is interpreted as the age of  $G_3$  deformation (Duguet et al. 2006). Other pegmatitic granites and pegmatites (including the Tanco pegmatite) in the belt have also been dated (Baadsgaard and Cerny 1993) returning similar results of  $2640 \pm 7$  Ma. These data are therefore consistent with field observations from this study that Tanco is emplaced along  $G_3$  fractures within gabbro. Given the nature of the deformation seen in the Oompa

Loompa pegmatite, it was sampled for U-Pb analysis to determine both its absolute age (for comparison to the “undeformed” Tanco pegmatite) as well as to constrain the age of the final increment of deformation along the NBLSZ. The data set resulted in the interpretation that the Oompa Loompa pegmatite has an age of crystallization of  $2647.4 \pm 1.0$  Ma, also consistent with regional deformation  $G_3$ . It becomes clear, therefore, that the Bernic Lake pegmatite group was emplaced during a belt-wide tectonomagmatic event synchronous with  $G_3$  deformation. Similar ages ( $2646.2 \pm 2.0$  Ma) and structural associations have been reported in the Separation Lake area (Larbi et al. 1999), which marks the eastern extension of the Bird River belt in Ontario.

### **5.3 Emplacement Model for the Bernic Lake Pegmatite Group**

Previous models for the emplacement of the Bernic Lake pegmatite group include: a) that it is hosted predominantly in a late, subhorizontal fracture set (Cerny et al. 1981), and b) that it is emplaced in a saddle-reef type dilation zone at the intersection of an  $F_1$ - $F_2$  fold interference (Vanstone, pers. comm.). As exposure of the pegmatite group is limited, these interpretations are based largely on the well-defined Tanco pegmatite and fail to explain the variability that exists in the style of emplacement across the entire suite of pegmatites. In the case of the former model, the flat-lying nature of the Tanco pegmatite and its occurrence along brittle fracture planes in the Tanco gabbro is indeed suggestive of late emplacement. Though as mentioned, the fractures hosting Tanco cannot be correlated with and are overprinted by extensive later fracture sets. Furthermore, this model does not account for the folding and boudinage observed in pegmatites to the east, the timing of which are synchronous with the Tanco pegmatite. As

for the latter model, the formation of a saddle-reef structure requires a discrete surface (i.e. a bedding plane) along which slip can occur during deformation, thus allowing for dilation. The Tanco pegmatite is hosted entirely within a relatively homogeneous, crystalline, subvolcanic intrusion, and the presence of such a surface within that lithology is tenuous. Furthermore, mapping by Gilbert (2005, 2006, 2007) has suggested that the Bernic Lake Formation represents a continuous, north-facing homoclinal sequence, which precludes the presence of local fold interference structural relationships.

On the basis of lithological and structural mapping bolstered by detailed U-Pb analyses, a syn-D<sub>3</sub> model that incorporates the many styles of emplacement observed in the Bernic Lake pegmatite group is proposed. The response to D<sub>3</sub> deformation around Bernic Lake occurs as a variety of structures (G<sub>3</sub> and G<sub>4</sub> structures) related to the nature of the lithologies affected. In mafic metavolcanic rocks, a prominent spaced S<sub>3</sub> cleavage consistently overprints the ubiquitous S<sub>2</sub> foliation. Along the NBLSZ, the S<sub>2</sub> foliation is reactivated as shear (C-) planes during (renewed) south-side-up dextral shearing, and in the Tanco gabbro, the response to D<sub>3</sub> strain is the formation of a conjugate fracture set. Since the Bernic Lake pegmatite group was emplaced during D<sub>3</sub>, it follows that the different emplacement styles and spatial distributions observed in the pegmatites are related to the heterogeneity in structural responses to D<sub>3</sub> strain by their respective host rocks. The difference in response to D<sub>3</sub> strain (from ductile G<sub>3</sub> structures to brittle G<sub>4</sub> structures) of the various lithologies is indicative of an emplacement depth of the Bernic Lake pegmatite group at or near the brittle-ductile transition.

Figure 27 shows a series of schematic diagrams illustrating the progression of deformation and pegmatite intrusion in the Bernic Lake area. North-south directed

shortening on volcanic and syn-volcanic rocks during  $D_2$  deformation resulted in the development of belt-scale isoclinal  $F_2$  folds in the volcano-sedimentary pile (Figure 27a). Continued compression resulted in strain accumulation, south-side-up shearing along the NBLSZ ( $G_2$ ) and the juxtaposition of various volcanic formations against one another (Figure 27b).  $D_3$  deformation caused preferential brittle-ductile reactivation along the NBLSZ and brittle deformation in rheologically competent units (i.e. conjugate fracture set in the Tanco gabbro). The reactivation along the NBLSZ created pathways through which granitic magma ascended from depth. In some instances (Oompa Loompa, Buck pegmatites), emplacement and crystallization occurred within dilational zones in the NBLSZ and the pegmatites record increments of  $D_3$  strain. In the case of the Tanco pegmatite, granitic melt escaped along the conjugate fracture system developed in the Tanco gabbro (Figure 27c). The Tanco pegmatite is by far the largest of the rare-element bearing pegmatites identified in the Bernic Lake pegmatite group. The model presented suggests that the fracture controls on the emplacement of the Tanco pegmatite may be in part responsible for its large dimensions. Increased fluid pressure along fracture planes created by intruding pegmatitic melt could have caused “unroofing” in the gabbro and formed the large space now occupied by the Tanco pegmatite (Figure 27c). U-Pb geochronological data from the pegmatites sampled in this study define, in part, a range of ages spanning ~ 2640-2652 Ma. This suggests that  $G_3$  deformation may have been ongoing during this timespan, and that multiple pulses of pegmatitic melt were continually emplaced over this period.

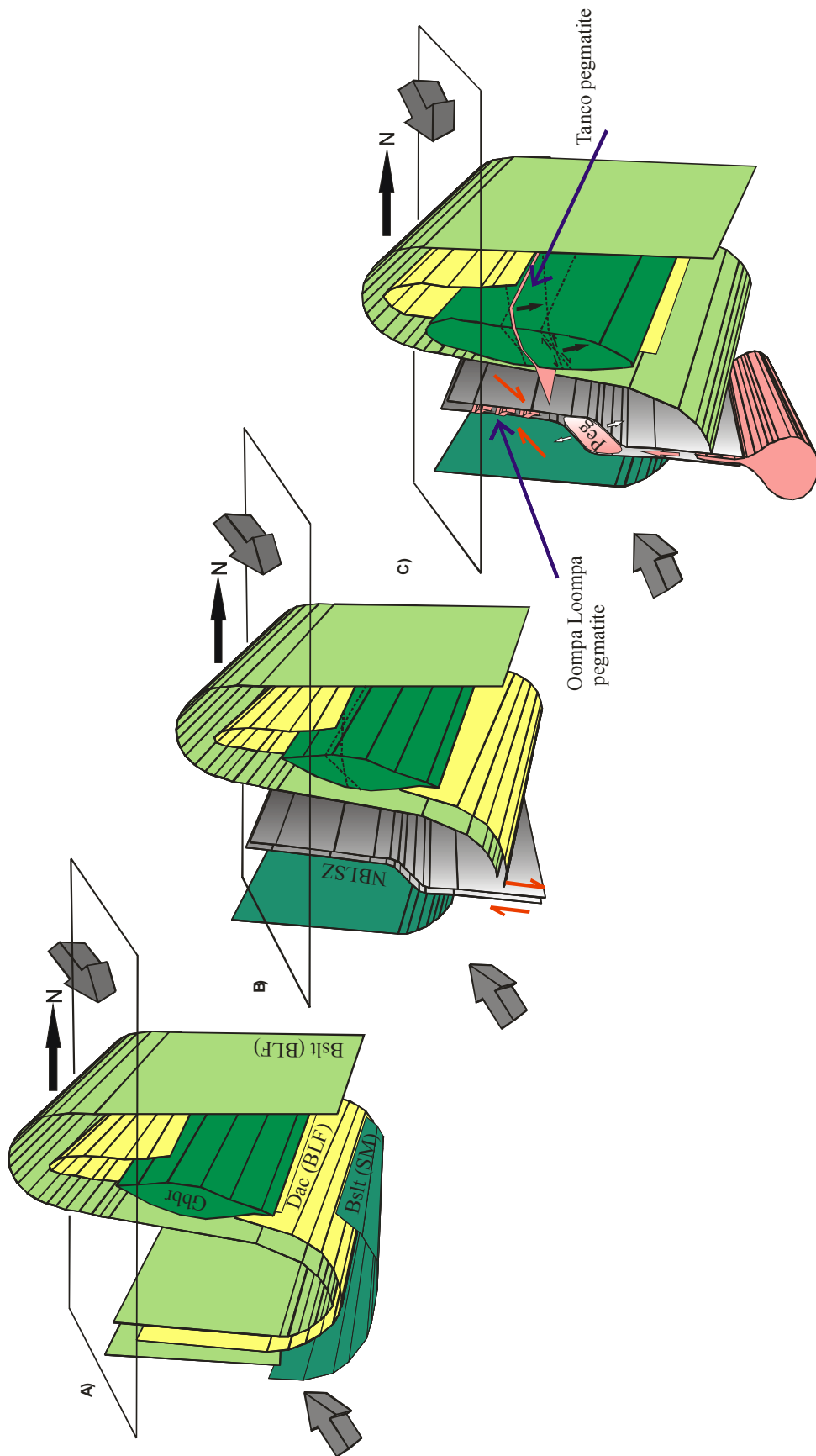


**Figure 27.** Schematic diagram showing the development of structures during  $G_{2-4}$  deformation and the emplacement of the Bernic Lake pegmatite group (see text for details). Abbreviations: BSLT (SM), south panel MORB-like basalt; Bstl (BLF), Bernic Lake Formation basalt; Dac (BLF), Bernic Lake Formation dacite; Gbbr, gabbro; Peg, pegmatite and pegmatitic melt; NBSZ, North Bernic Lake shear zone. Large arrows represent principal shortening axes during progressive  $G_{2-4}$  deformation, horizontal plane represents current surficial expression, dashed lines in gabbro represent brittle fractures.

## 5.4 Summary

Examination of rocks exposed around Bernic Lake reveal a complex deformation history related to the amalgamation of the Superior Province that occurred episodically between *ca.* 2.72 – 2.64 Ga. Close investigations of the rare element-bearing Bernic Lake pegmatite group indicates that it was emplaced during a belt-wide tectonomagmatic event in the final stages of D<sub>3</sub> deformation (between 2.65 and 2.64 Ga) and that the pegmatitic melt used reactivated belt-scale shear zones as conduits for ascent into the upper crust. Pegmatites crystallized within both the shear zones themselves and in adjacent lithologies. The style of pegmatite emplacement (shear- versus fracture-hosted) was determined by the different responses to strain of the various host lithologies to this deformation event. Structural controls on pegmatite emplacement can be integrated into current exploration practices (e.g. surficial geochemical anomalies) for rare element-bearing pegmatites and allow for more comprehensive exploration models. Given the controls on emplacement, obvious targets exist along the NBLSZ and other belt-scale structures. In particular, however, locations where the orientation of these structures is favourable for dilation (releasing bends or jogs), either at surface or at depth, thereby allowing more room for pegmatitic melt, should be considered more prospective areas. Furthermore, as with the Tanco pegmatite, areas where rheologically competent lithologies occur along or adjacent to these structures should also be considered as potential areas for widespread intrusion.

## References

- Beakhouse, G.P. 1977. A subdivision of the western English River subprovince; Canadian Journal of Earth Sciences **14**. pp. 1481–1489.
- Brisbin, W.C. 1986. Mechanics of pegmatite intrusion. American Mineralogist **71**. pp. 644-651.
- Card, K.D. 1990. A review of the Superior Province of the Canadian Shield, a product of Archean accretion. Precambrian Research **48**: 99-156.
- Card, K.D. and Ciesielski, A. 1986. Subdivisions of the Superior Province of the Canadian Shield. Geoscience Canada **13**: 5-13.
- Cerny, P. 1972a. The Tanco pegmatite at Bernic Lake Manitoba. VII, Eucryptite. Canadian Mineralogist **11**. pp. 708-713.
- Cerny, P. 1972b. The Tanco pegmatite at Bernic Lake Manitoba. VIII, Secondary minerals from the spodumene-rich zones. Canadian Mineralogist **11**. pp. 714-726.
- Cerny, P. 1974. The present status of the analcime-pollucite series. Canadian Mineralogist **12**. pp. 334-341.
- Cerny, P. 1978. Alteration of pollucite in some pegmatites of southeastern Manitoba. Canadian Mineralogist **16**. pp. 89-95.
- Cerny, P. 1990. Distribution, affiliation and derivation of rare-element granitic pegmatites in the Canadian Shield. Geologische Rundschau **79/2**. pp. 183-226.

- Cerny, P. 1991. Fertile granites of Precambrian rare-element pegmatite fields: is geochemistry controlled by tectonic setting or source lithologies? *Precambrian Research* **51**. pp. 429-468.
- Cerny, P. and Bristol, N.A. 1972. New mineral occurrences in pegmatites of southeastern Manitoba. *Canadian Mineralogist* **11**. pp. 560-563.
- Cerny, P., Fryer, B., Longstaffe, F., and Tammemagi, H. 1987. The Archean Lac du Bonnet Batholith, Manitoba: Igneous history, metamorphic effects, and fluid overprinting. *Geochimica et Cosmochimica Acta* **51**. pp. 421-438.
- Cerny, P. and Trueman, D.L. 1977. Petrogenesis of pegmatites in the Cat Lake-Winnipeg River area. Centre for Precambrian Studies, University of Manitoba, Annual Report 1976. pp. 26-32.
- Cerny, P., Trueman, D.L., Ziehlke, D.V., Goad, B.E., and Paul, B.J. 1981. The Cat Lake-Winnipeg River and the Wekusko Lake pegmatite fields, Manitoba. Manitoba Department of Energy and Mines, Mineral Resources Division. Economic Geology Report ER80-1. 215 pp.
- Cerny, P. and Turnock, A.C. 1971b. Pegmatites of southeastern Manitoba. Geological Association of Canada, Special Paper **9**. pp. 119-127.
- Cerny, P. and Turnock, A.C. 1971a. Niobium-tantalum minerals from granitic pegmatites at Greer Lake, southeastern Manitoba. *Canadian Mineralogist* **10**. pp. 755-772.
- Cerny, P. and Turnock, A.C. 1971c. Beryl from granitic pegmatites at Greer Lake, southeastern Manitoba. *Canadian Mineralogist* **13**. pp. 55-61.

- Cruden, A.R., Davis, D.W., Menard, T., and Robin, P.-Y. R. 1997. Structural and geochronological relationships between the Winnipeg River and Wabigoon subprovinces: implications for the terrane accretion model. *In* Western Superior Transect. Lithoprobe Secretariat, University of British Columbia, Vancouver, B.C. Lithoprobe Report 63. pp. 18-26.
- Davies, J.F. 1952. Geology of the Oiseau (Bird) River area, Lac du Bonnet Mining Division. Manitoba Mines Branch Publication 51-3. 24 pp.
- Davies, J.F. 1955. Geology and mineral deposits of the Bird Lake area. Manitoba Mines Branch Publication 54-1. 44 pp.
- Davies, J.F. 1956. Geology of the Booster Lake area, Lac du Bonnet Mining Division. Manitoba Mines Branch Publication 55-1. 15 pp.
- Davies, J.F. 1957. Geology of the Winnipeg River area (Shatford Lake-Ryerson Lake), Lac du Bonnet Mining Division. Manitoba Mines Branch Publication 56-3. 27 pp.
- Davis, D.W. 2008. Sub-million-year age resolution of Precambrian igneous events by thermal extraction–thermal ionization mass spectrometer Pb dating of zircon: Application to crystallization of the Sudbury impact melt sheet. *Geology* **36/5**. pp. 383-386.
- Duguet, M., Lin, S., Gilbert, H.P. and Corkery, M.T. 2005. Preliminary results of geological mapping and structural analysis of the Bird River greenstone belt, southeastern Manitoba (NTS 52L5 and 6). *In* Report of Activities 2005, Manitoba Industry, Economic Development and Mines, Manitoba Geological Survey, pp. 117–124.
- Duguet, M., Gilbert, H.P., Corkery, M.T. and Lin, S. 2006. Geology and structure of the Bird River Belt, southeastern Manitoba (NTS 52L5 and 6). *In* Report of Activities

2006, Manitoba Science, Technology, Energy and Mines, Manitoba Geological Survey, pp. 170–183.

Duguet, M., Lin, S., Gilbert, H.P. and Corkery, M.T. 2007. Structural geology and kinematic evolution of the Bird River greenstone belt, English River Subprovince, Manitoba (NTS 52L5, 6). *In* Report of Activities 2007, Manitoba Science, Technology, Energy and Mines, Manitoba Geological Survey, pp.144–154.

Gilbert, H.P. 2005. Geological investigations in the Bird River area, southeastern Manitoba (parts of NTS 52L5N and 6N). *In* Report of Activities 2005, Manitoba Industry, Economic Development and Mines, Manitoba Geological Survey, pp. 125–139.

Gilbert, H.P. 2006. Geological investigations in the Bird River area, southeastern Manitoba (NTS 52L5N and 6). *In* Report of Activities 2006, Manitoba Science, Technology, Energy and Mines, Manitoba Geological Survey, pp. 184–205.

Gilbert, H.P. 2007. Stratigraphic investigation in the Bird River greenstone belt, Manitoba (part of NTS 52L5, 6). *In* Report of Activities 2007, Manitoba Industry, Economic Development and Mines, Manitoba Geological Survey, pp. 129-143.

Hrabi, R.B. and Cruden, A.R. 2006. Structure of the Archean English River subprovince: implications for the tectonic evolution of the western Superior Province, Canada. *Canadian Journal of Earth Sciences* **43**. pp. 947-966.

Kremer, P.D. 2005. Preliminary results from geological mapping of the Bernic Lake Formation, Bird River greenstone belt, southeastern Manitoba. *In* Report of Activities 2005, Manitoba Industry, Economic Development and Mines, Manitoba Geological Survey, pp. 140–145.

- Kremer, P.D. and Lin, S. 2006. Structural geology of the Bernic Lake area, Bird River greenstone belt, southeastern Manitoba (NTS 52L6): implications for rare element pegmatite emplacement. *In* Report of Activities 2006, Manitoba Science, Technology, Energy and Mines, Manitoba Geological Survey, pp. 206–213.
- Larbi, Y., Stevenson, R., Breaks, F., Machado, N., Gariépy, C., 1999. Age and isotopic compositions of late Archean leucogranites: implications for continental collision in the western Superior Province. *Canadian Journal of Earth Sciences*, **36**: 495–510.
- Lenton, P.G. 1979. Mineralogy and petrology of the Buck claim lithium pegmatite, Bernic Lake, southeastern Manitoba. Unpublished M.Sc. thesis, Department of Earth Sciences, University of Manitoba. 164 pp.
- McRitchie, W.D. The petrology and environment of the acidic plutonic rocks of the Wanipagow-Winnipeg River region, southeastern Manitoba. Manitoba Mines Branch, Publication **71-1**. pp. 7-61.
- Mealin, C.A. 2005. Geological investigations of the Chrome property, Bird River Sill, southeastern Manitoba (NTS 52L5). *In* Report of Activities 2005, Manitoba Industry, Economic Development and Mines, Manitoba Geological Survey, p. 146–149.
- Mealin, C.A. 2006. Geological investigations in the Bird River Sill, southeastern Manitoba (part of NTS 52L5): geology and preliminary geochemical results. *In* Report of Activities 2006, Manitoba Science, Technology, Energy and Mines, Manitoba Geological Survey, pp. 214–225.
- Mealin, C.A. 2008. Geology, geochemistry and Cr-Ni-Cu-PGE mineralization of the Bird River sill: Evidence for a multiple intrusion model. Unpublished M.Sc. thesis, Department of Earth Sciences, University of Waterloo. 155 pp.

- Melnyk, M.J., Davis, D.W., Cruden, A.R., and Stern, R.A. 2006. U-Pb ages constraining structural development of an Archean terrane boundary in the Lake of the Woods area, western Superior Province, Canada. *Canadian Journal of Earth Sciences* **43**. pp. 967-993.
- Moore, E.S. 1913. Region east of the south end of Lake Winnipeg. Geological Survey of Canada, Summary Report, 1912. pp. 31-43.
- Morgan, G.B. IV and London, D. 1987. Alteration of amphibolitic wallrocks around the Tanco rare-element pegmatite, Bernic Lake, Manitoba. *American Mineralogist* **72**. pp. 1097-1121.
- Peck, D.C. and Theyer, P. 1998: PGE-copper-nickel potential of mafic-ultramafic intrusions in the Bird River greenstone belt (parts of NTS 52L); *in* Report of Activities 1998, Manitoba Energy and Mines, Manitoba Geological Survey, p. 151-160.
- Percival, J.A., Sanborn-Barrie, M., Skulski, T., Stott, G.M., Helmstaedt, H., and Davis, D.W. 2006. Tectonic evolution of the western Superior Province from NATMAP and Lithoprobe studies. *Canadian Journal of Earth Sciences* **43**. pp. 1085-1117.
- Springer, G.D., 1949. Geology of the Cat Lake-Winnipeg River area. Manitoba Mines Branch, Preliminary Report 48-7. 28 pp.
- Springer, G.D. 1950. Mineral Deposits of the Cat Lake-Winnipeg River area, Lac du Bonnet Mining Division. Manitoba Mines Branch, Publication 49-7. 14 pp.
- Theyer, P. 1990: Petrography, chemistry and distribution of platinum and palladium in ultramafic rocks of the Bird River Sill, SE Manitoba, Canada; *Mineralium Deposita*, v. 26, p. 165-174.

- Theyer, P., Bruni, E. and Sundell, C. 2001: Stratigraphy, geology and mineralization of selected parts of the Page property, Bird River Sill (part of NTS 52L/5); *in* Report of Activities 2001, Manitoba Industry, Trade and Mines, Manitoba Geological Survey, p. 126–132.
- Thurston, P.C., Osmani, I.A., and Stone, D. 1991. Northwestern Superior Province: Review and terrane analysis. *In* Geology of Ontario. *Edited by* P.C. Thurston, H.R. Williams. R.H Sutcliffe, and G.M. Stott. Ontario Geological Survey Special Vol. 4, Part 1. pp. 138-141.
- Trueman, D.L. 1980. Stratigraphic, structural, and metamorphic petrology of the Archean greenstone belt at Bird River, Manitoba. Ph.D. thesis, Department of Earth Sciences, University of Manitoba. 155 pp.
- Turek, A., Keller, R., Van Schmus, W.R., and Weber, W. 1989. U-Pb zircon ages for the Rice Lake area, southeastern Manitoba. *Canadian Journal of Earth Sciences* **26**. pp. 23-30.
- Tyrrell, J.B. 1900. East shore, Lake Winnipeg. Geological Survey of Canada, Annual Report, 1898. Vol. 11, part G.
- Vanstone, P., Young, S., Galeschuk, C., Simard, R., and Gibb, A. 2002. The Tanco rare-element pegmatite, southeastern Manitoba. 21 pp.
- Van Lichtervelde, Salvi S., and Béziat D. 2007. Textural features and chemical evolution in tantalum oxides: magmatic vs. hydrothermal origins for Ta mineralization in the Tanco lower pegmatite, Manitoba, Canada. *Economic Geology* **102**. pp. 257-276.
- Wang, X. 1993. U-Pb zircon geochronology study of the Bird River greenstone belt, southeastern Manitoba. M.Sc. thesis, University of Windsor, Windsor, Ontario, 96 pp.